Post print author.

Acceptance date by *Hydrogeology Journal*: 17 February 2026

Propagation of agricultural and sewage nitrate in a chalk aquifer through regional numerical modelling of groundwater flow and solute transport in the Mons Basin, Belgium

Louis Christiaens[1,2], Guillaume Vandelois[1], Serge Brouyère[2], Philippe Orban[2], Catherine SOHIER[3], Aurore Degré[3], Pascal Goderniaux[1*]

[1] University of Mons – Polytech Mons – Geology and Applied Geology, Mons, Belgium

[2] University of Liège – Urban and Environmental Engineering – Hydrogeology and Environmental Geology, Liège, Belgium

[3] University of Liège, TERRA teaching and research centre, Gembloux Agro-Bio Tech, Gembloux, Belgium

*Corresponding author: Prof. Pascal GODERNIAUX – Pascal.Goderniaux@umons.ac.be

Abstract

This study tackles the nitrate pollution of groundwater in a chalk aquifer (Mons Basin, Belgium) using a numerical modelling approach based on MODFLOW 6 and Flopy. Previous research focused on hydrogeochemical surveys and isotopic measurements in this area has revealed the implication of diverse anthropogenic sources (mineral fertilizer, manure and sewage) explaining nitrate contamination. Using numerical modelling, this research studies and demonstrates how the pollutant migrates through the saturated aquifer. A 3D multi-layer steady-state model is developed to simulate the regional mean groundwater flow in the aquifer. A transient solute transport component is coupled to the steady state flow model. The MODFLOW 6 model inputs included simulated results from the EPIC GRID hydrological model, which calculates the amount of nitrogen of agricultural origin reaching the saturated groundwater, and hypothetical nitrate leakages from the sewage network. The model was calibrated to historical piezometric levels and nitrate concentrations, and used for predictive purposes between 2023 and 2050, using six different scenarios of diffuse agricultural inputs. The scenarios included three climate scenarios coupled with two agricultural practice scenarios. The model was also used to simulate the potential impact of addressing the contamination by sewage. Although the number of scenarios remains limited, results generally showed a higher influence of the climate scenarios considered compared to the tested changes in agricultural practices. A more exhaustive range of scenarios remains to be tested, but the developed numerical model remains efficient and flexible to address the questions related to regional scale nitrate contamination.

1. Introduction

Mainly driven by the development and widespread use of fertilizers during the second half of the 20th century (Singh and Sekhon, 1979; Spalding and Exner, 1993; Strebel et al., 1989), nitrate contamination of aquifers continues to threaten the integrity of drinking water reserves worldwide (Abascal et al., 2022; Craswell, 2021; Erisman et al., 2013). Beyond its impact on groundwater quality, excessive nitrogen input into aquatic environments contributes to eutrophication (Smith et al., 1999; Vitousek et al., 1997). It also constitutes a health hazard for humans when ingested, causing an increased risk of cancer (Canter, 2019; Sandor et al., 2001), and potentially leading to cases of methemoglobinemia if consumed by infants (Fan and Steinberg, 1996). To limit such health risks, the World Health Organization (WHO) considers a maximum acceptable nitrate concentration of 50 mg/L in drinking water (WHO, 2017).

In addition to characterizing nitrate pollution and understanding the associated processes across various spatial and temporal scales, the need for modelling is also crucial. It allows the confrontation of hypotheses through physically based simulations and the investigation of parameter sensitivities. Modelling is also important for predictive purposes, particularly for the management of groundwater resources at the basin or aquifer scale. It can be used to forecast the effectiveness of mitigation measures or the impact of external stresses such as climate change.

Several studies have addressed groundwater contamination in nitrate by developing numerical models combining groundwater flow with solute transport, at medium to large scales. Lee et al. (2006) used the MODFLOW finite difference computational code (McDonald and Harbaugh, 1988) to simulate flow, coupled with the reactive transport code RT3D (Clement, 1999), allowing them to simulate nitrification/denitrification processes. Their study focused on a relatively localized domain (160×28×20 m) and compared simulated results with field measurements over a period of 1000 days. In this model, nitrate was input into the simulation through a boundary condition with a constant concentration in a source zone. Orban et al. (2010) developed a numerical flow and transport model based on the hybrid finite element mixing cell method to simulate the impact of a change in nitrate inputs in the chalk aquifer of the Geer Basin (Belgium). The model integrates both the fully saturated and the thick partially saturated zones, where flow and transport processes are determinant. This model integrates scenarios with linear nitrate inputs from agricultural sources and predicted response times ranging from 5 to 50 years for a reversal of nitrate concentrations trends, considering adapted fertilizer spreading plans. This groundwater modelling approach was also coupled with a socio-economic analysis, illustrating the cost-effectiveness of the proposed mitigation measures (Hérivaux et al., 2008). In Egypt, Eltarabily et al. (2017) used a coupled MODFLOW and MT3D model to simulate nitrate propagation in the central part of the Nile Delta aquifer. This model allowed identifying the most nitrate-affected zones and proposed strategies to optimize groundwater use, while highlighting the importance of limiting nitrate leaching in the area. In this study, the nitrate concentrations in recharge is deduced from the quantities of fertilizers applied and the recharge volumes during the fertilization period. Zhang et al. (2019) also developed a flow and transport model based on MODFLOW and MT3DMS codes to investigate nitrogen contamination of an aquifer in southwest of China. Nitrate inputs were calculated based on a cartographic analysis of land use, fertilizer application frequencies, rainfall, depth to the top of the saturated zone, and standard fertilizer quantities used by crop type. After calibration with field measurements, the model was used to simulate the impact of various land-use change scenarios on future nitrate concentrations over a 640 km² area discretized using 0.09 km² cells). Wei et al. (2019) combine nitrate percolation in the partially saturated zone using the SWAT model (Soil and Water Assessment Tool) with a MODFLOW groundwater flow model and a RT3D reactive transport model. The main objective of this study is to use a combination of these three tools to determine nitrate exchange (loading/unloading) between the Sprague River and the underlying aquifer (USA). Karlović et al. (2022) developed a regional flow and transport model of an alluvial aquifer in the Varaždin region (Croatia)

using the MODFLOW and MT3DMS codes. For this model, the authors imposed a fixed nitrate input rate for each land use class identified using the Corine Land Cover (EEA, 2018). They simulated the impact of different nitrate input scenarios over a 20-year period to assess the relative influence of agricultural practices and wastewater pollution on nitrate concentrations. Given the uncertainty about the location of sewage network leaks and the nitrogen concentration in wastewater, a constant nitrate concentration of 25 mg/L was applied in urbanized areas inputs. Finally, Paradis et al. (2016) investigated the impact of climate change on nitrate concentrations in Prince Edward Island (Canada) up to 2050. They developed a large-scale, regional flow and solute transport model (5660 km²) using the FEFLOW finite element code, with triangular elements of about 0.0925 km². The study concluded that the future increase in nitrate concentrations on the island (between 25 and 32% depending on the scenarios considered) will result from both the progressive attainment of steady-state conditions related to the current nitrogen loadings and from additional agricultural nitrogen inputs driven by changing climatic conditions.

Modelling nitrate contamination in groundwater at relatively large scales remains complex and challenging. The spatial and temporal resolutions required, combined with the need to accurately represent heterogeneous aquifer systems, often impose constraints that do not align with the scale of agricultural pressures. At the regional scale, the inclusion of multiple nitrate sources is not always implemented, either due to data limitations or because it introduces additional complexity. Nevertheless, this consideration is critical for assessing the effectiveness of mitigation strategies in mixed rural, urban, and industrial environments. Finally, although several previous studies assess the effect of climate change on nitrate concentrations (i.e. Focaccia et al. (2021); Rotiroti et al. (2023); Sarkar et al. (2022), Stuart et al.(2011)), this impact remains difficult to quantify and is often not included in management policies. Given the potentially long groundwater transit times and the delayed response to mitigation measures, it is however relevant to address all issues simultaneously.

In this context, this study discusses the development and use of a numerical regional 3D groundwater flow and transport model to simulate the fate of nitrate in the chalk aquifer of the Mons Basin (~400 km²). Located in the southern part of Belgium and affected by nitrate contamination (Christiaens et al., 2023), this aquifer is strategic for the production of drinking water for local consumption and for export to Brussels City and Flanders. This study pursues several specific objectives related to different questions. (1) It aims to represent flow and nitrate transport at the scale of the chalk aquifer saturated zone, considering the whole heterogeneity of the hydrogeological environment and including contrasted lithologies and geometries, unconfined recharge areas upstream and the partially confined zones downstream. It is also intended to assess and discuss the sensitivity of nitrate concentrations to the model parameters and stresses. (2) The approach intends to integrate in the simulations different nitrate sources, their spatial and time distributions, including agricultural fertilizers and sewer network leakage. Scenarios are based on the works of Christiaens et al. (2023) who previously studied the sources and fate of nitrate pollution in this aquifer. (3) Finally, this study also seeks to provide and discuss a methodology to evaluate the impact of climate change, agricultural practices and restoration works on the wastewater system on the nitrate concentrations in the aquifer. Predictions over the next 25 years are made based on a selection of scenarios.

To reach those objectives, the modelling approach applied here is based on the development of a regional steady-state groundwater flow model, coupled with a transient solute transport model. The latest version of the MODFLOW6 computational code (Langevin et al., 2017a) is used. Although the past versions of the MODFLOW and MT3DMS codes have been widely used in the past for studying groundwater nitrate contamination, applications with MODFLOW 6 are much less frequent. It was nevertheless chosen for three main reasons: (1) It is compatible with an unstructured grid, which allows representation of the wedge-shaped geological layers forming the aquifer and which may easily be refined locally where required. (2) It is developed and structured to facilitate the coupling of flow and transport in combined simulations. (3) It allows integrating and upgrading previous models of the Mons Basin chalk aquifer

(ex. Rorive and Van Wittenberge, 2004), some of them being very old and outdated. By using the recent and versatile calculation code MODFLOW6, the objective is here to create a flexible and adaptable tool for addressing various challenges in an aquifer intensively exploited for drinking water production.

The development of the solute transport simulation requires information on the quantities of nitrogen applied in agricultural production areas and entering into the aquifer, in the past and in the future. This information is generally not easy to collect or calculate (Di and Cameron, 2002), but is actually crucial to perform rigorous calibration of the model and provide robust and realistic projections. In this study, the groundwater flow and transport MODFLOW model is coupled with simulated outputs from the physically based, spatially distributed hydrological model EPIC GRID (Sohier and Degre, 2010) derived from the original field-scale "erosion-productivity impact calculator" (EPIC) model (Williams et al, 1984). The EPIC GRID model considers the amount of fertilizer applied, weather conditions and crop type, soil – plant – water interactions and simulates the amount of nitrogen leaching to the saturated zone according to historical operations in South Belgium, or specific scenarios. In this study, the predictive results of the EPIC Grid model in six different scenarios are used. These were obtained using three regional meteorological scenarios corresponding to cold, medium and warm climate evolution trends up to 2050 (Wyard et al., 2017), combined with two agricultural practice scenarios (Baret et al., 2019).

The chalk aquifer of the Mons Basin section of this study describes the geological and hydrological contexts of the Mons Basin chalk aquifer, as well as available data and previous characterization works. The ***Model development*** section presents the conceptual assumptions, the mathematical models, the spatial and time discretization schemes, parametrization, and the results of the sensitivity analysis and calibration procedures. The ***Modelling of future nitrate concentrations*** section describes the different scenarios used in this study (sewage network, agricultural practices and climate change) and the results of their application in the groundwater flow and transport model. The ***Discussion*** section discusses the findings regarding the impact of those drivers on nitrate concentrations in the aquifer. It also addresses the challenges, limitations and perspectives of the applied methodology with the aim of making a meaningful contribution to nitrate modelling and management at the scale of groundwater bodies.

2. The chalk aquifer of the Mons Basin

The modelled chalk aquifer is located in the southern part of Belgium, covers an area of over 400 km², and is part of the Mons Sedimentary Basin (Figure *1*(a)). Due to its formation in a subsiding Cretaceous basin, the thickness of the aquifer varies, from a maximum of 350 m in the center, to a few meters on the edges of the Basin (Figure *1* (b), Mengeot et al., 2017a). Mainly composed of Mesozoic chalk, the aquifer also includes levels of calcarenite and tuffeau at the top of the chalk series and marly units at the base. While the chalk outcrops on the northern and southern edges of the basin, the inner part of the aquifer is partially confined under different layers of Cenozoic sands and clays, overlain by alluvium in the center of the area. The confined areas of the aquifer cover up to 40% of its total surface (Rorive and Goderniaux, 2014). The chalk aquifer is embedded in less permeable geological formations: to the north, Upper Carboniferous (Namurian) pelites and sandstones; to the east, Upper Carboniferous (Whestphalian) schisto-sandstone; and Devonian quartzopelites to the southeast. The western boundary of the studied area corresponds to the national border with France. Groundwater recharge occurs mainly in the unconfined parts of the aquifer on the northern and southern areas of the Basin. The observed piezometric levels, shown in Figure *1*(a), generally follow the topographic levels and indicate the main groundwater flow directions. The Haine River and main tributaries drain most of the groundwater in the chalk aquifer, in addition to the volumes abstracted. A relatively small quantity of groundwater flows westward across the Belgium – France border.

As presented in Mengeot et al. (2017a), although the chalk matrix is characterized by low permeability, the hydraulic conductivity in the aquifer is significantly higher due to the presence of fractures. It varies depending on depth, spatial location within the basin and the degree of chalk fracturing. Pumping tests carried out in the chalk aquifer classically give hydraulic conductivity values ranging from 10^{-6} to 10^{-3} m/s (Rorive and Goderniaux, 2014; SWDE, 2002). As a general rule, hydraulic conductivity is the highest in the center of the aquifer, where the sequence of chalk layers is thicker. The more marly chalk observed at the base of the aquifer and outcropping along the edges of the basin shows a lower hydraulic conductivity (Rorive and Van Wittenberge, 2004).

The production of drinking water, for domestic and industrial use, represents the largest term of the aquifer water balance. Every year, a total of approximately 50 million m³, representing about 60% of the estimated recharge, is extracted by the three water public companies operating in the region, as well as by industries and private wells. The produced drinking water is distributed locally or exported, mainly to Brussels City. Figure *1*(c) shows the locations of the main active water production wells.

Land use is mixed and heterogeneous over the area, ranging from open fields dedicated to agriculture in the south to a densely urbanized area in the center. This variety of land use multiplies the potential sources of anthropogenic nitrate threatening groundwater quality, including mineral fertilizers, manure and sewage leakage over the chalk aquifer (Christiaens et al. (2023). In addition, the industrial and mining past history of the region has scattered waste mining heaps across the territory. Sometimes converted into landfill sites, they also represent potential pollution hotspots and locally increase nitrogen concentrations.

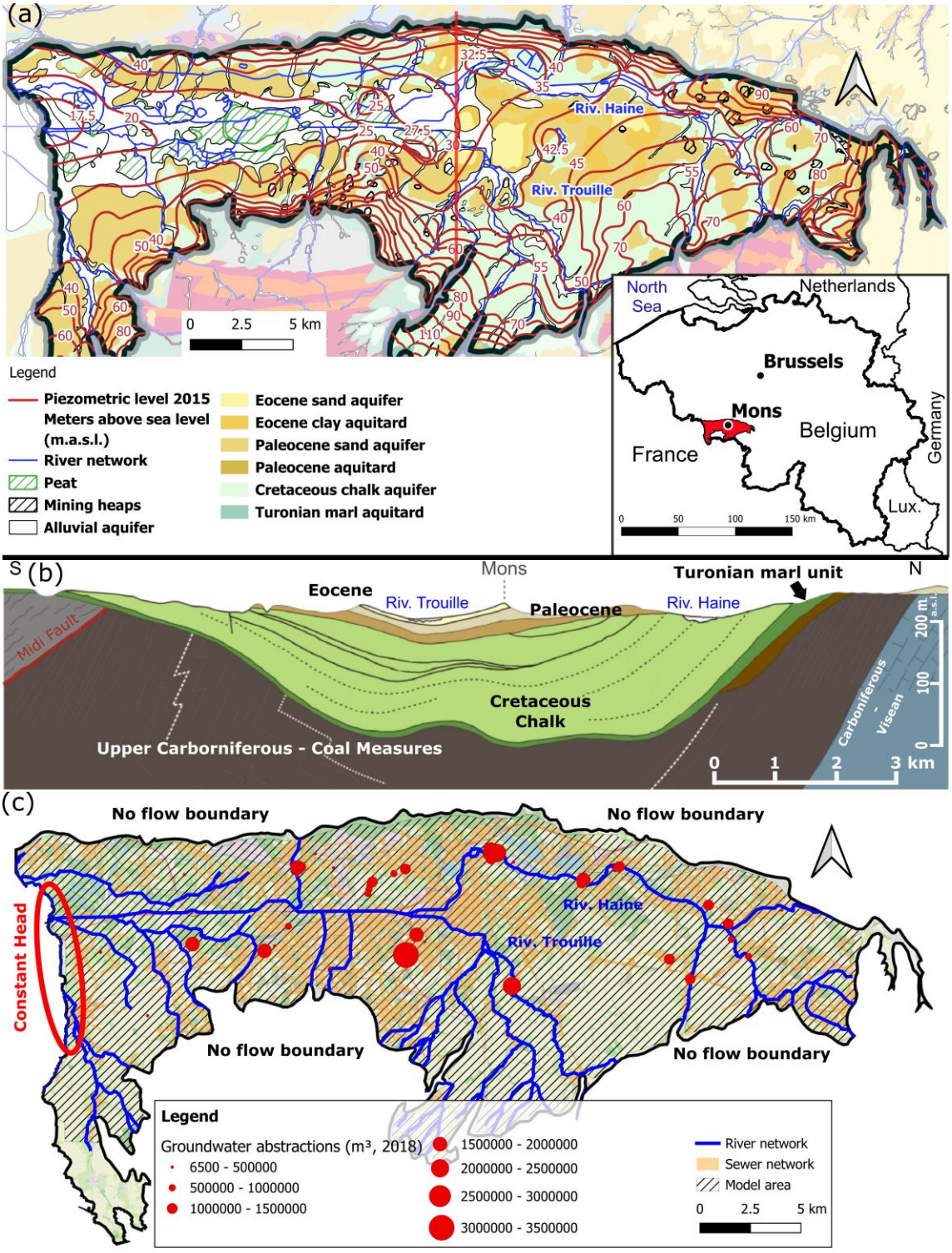

Figure 1: a) Hydrogeological map of the Mons Sedimentary Basin (Bastien et al., 2017; Bougard et al., 2017; Habils et al., 2017a, 2017b; Mengeot et al., 2017b) and piezometric levels (2015). b) Geological vertical cross-section with location indicated by the red line on map (a) (modified from Pirson et al., 2008). c) Location of the elements used and described in the conceptual model, including the locations of the water production wells with annual abstracted volumes, the constant head boundary condition and the river/sewer networks.

The geometry of the geological layers, used to build the model grid, is provided by Dupont (2021), Marliere (1967) and Rorive and Van Wittenberge (2004). It includes the lateral and vertical limits of the alluvial deposits, the Ypresian (Eocene) and Thanethian (Paleocene) sands and clays, and the whole

sequence of geological formations constituting the chalk aquifer. Piezometric data are collected by the regional public administration (SPW) and the Polytechnic Faculty (University of Mons). A full piezometric map is available for May 2015 (Figure *1* (a)). Hydrochemical datasets are available from databases of the public administration and water companies (SPW, Ressources naturelles et Environnement, 2019), as well as from two sampling campaigns performed in 2020 and 2021 by Christiaens *et al.* (2023). They include the concentrations of major elements and ions regularly quantified by drinking water producers at production wells. These datasets spatially cover most of the studied area and provide information about the temporal evolution of nitrate concentrations in the main production wells.

In terms of nitrate contamination in the aquifer, 76% of regular quality monitoring points show concentrations above the recommended limit for ecosystem protection (25 mg/l) (Gouvernement Wallon, 2016; SPW and DEE, 2022). 14% of these sampling points present a concentration above the drinking water standard of 50 mg/L (WHO, 2017). The rise in nitrate concentrations began in the second half of the 20th century, following the progressive use of fertilizers. Figure *2* shows the concentrations measured at six production wells between 1990 and 2020. Although not all production wells currently exceed the drinking water standard, the overall trend in nitrate concentration is upwards and justifies measures to preserve the sustainability of the most important drinking water production sites.

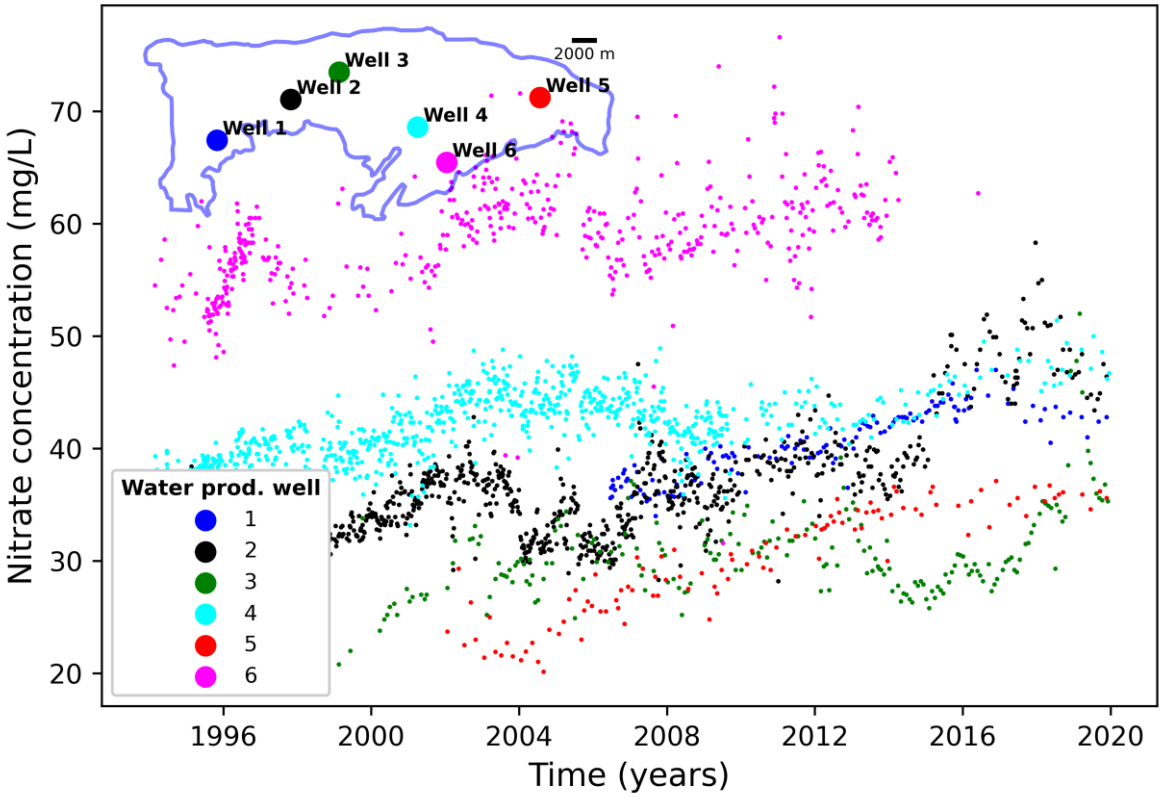

Figure 2: Nitrate concentrations observed at different water production wells from 1990 to 2020 (SPW, Ressources naturelles et Environnement, 2019). Water prod. well: water production well.

Christiaens et al. (2023) conducted a global study on nitrate pollution of this aquifer, relying on two sampling campaigns carried out at production wells, piezometers and traditional wells distributed across the aquifer (Figure *3*). Collected data in a total of 72 locations include values of physicochemical parameters, concentrations of significant elements and ions, nitrogen species, as well as isotopic analyses of nitrate ($\delta^{15}N$ and $\delta^{18}O - NO_3^-$) and boron ($\delta^{11}B$) in groundwater. In combination with multi-criteria analyses, including principal component analysis (PCA) and t-distributed stochastic neighbor embedding (t-SNE, van der Maaten and Hinton (2008)), these data were used to identify and

spatialize different types of nitrate sources on the chalk aquifer, as shown in Figure *3*. In particular, groups of samples are clearly influenced by manure application (Group A) and mineral fertilizers (Group B), mainly used in the southern agricultural areas. In the center of the studied area and beneath the most urbanized zones, results highlight groundwater contamination by wastewater from the sewage system (Group C). Group D presents a mixed signature between mineral fertilizer, manure and sewage. Several locations situated beneath Quaternary alluvial and Tertiary clayey deposits show no detectable nitrate due to denitrification processes. Further details on these groups and the methodology are provided in Christiaens et al. (2023). Nitrate concentration values, as well as their classification into distinct groups, are subsequently used in the model calibration process (see the ***Model development*** section).

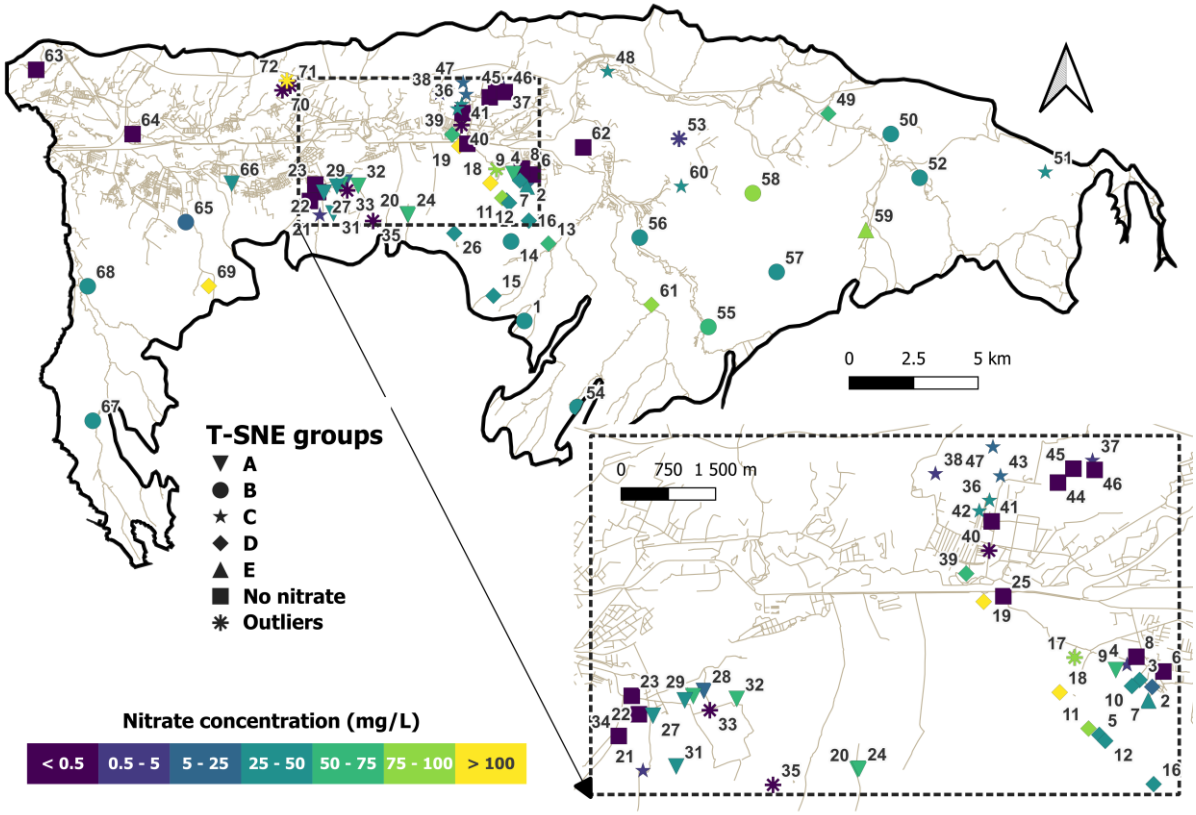

Figure 3: Nitrate concentrations measured during the 2020 and 2021 campaigns performed by Christiaens et al. (2023). Color code corresponds to lab quantified nitrate concentrations while the symbols indicate the statistical group assigned to each sampling point, based on a t-SNE dimensional reduction analysis (Christiaens et al., 2023). Group A: 'manure' signature; Group B: 'mineral fertilizer' signature; Group C: 'sewage' signature, Group D: 'mixed' signature. Group E does not present a clear signature and contains sampling points impacted by local pollution.

3. Model development

The control-volume finite difference MODFLOW 6.3.0 calculation code is used for modelling. Coupled with the python package Flopy (Bakker et al., 2023, 2016), this fully open-source framework allows for the simulation of groundwater flow (Langevin et al., 2017b) and solute transport (Langevin et al., 2022) processes within the same simulation. Results are then post-processed using a combination of Flopy and Python 3 scripts. The main improvements in MODFLOW 6 compared with previous versions include: the ability to combine several different nested models with separated grids and model types in a single simulation (Langevin et al., 2024), support for unstructured mesh grids, and the ability to define zero-thickness cells while maintaining vertical flow continuity thanks to the 'flow through cells' capability (Langevin et al., 2017a).

3.1. Mesh and flow conceptual modelling

Given the relatively complex geological structure of the study area, constructing the model grid represents a challenging task. It was decided to adopt a layered vertex grid approach ("disV", in Langevin et al. 2017b). Thanks to the "flow through cell" concept implemented in this version of MODFLOW 6, wedge-shaped cell layers, reflecting the geometry of this hydrogeological basin, are implemented in areas where the total aquifer thickness decreases, and geological units tend to thin out and disappear.

From a horizontal perspective, the geographical limits of the model follows the physical boundaries of the chalk aquifer, with the exception of a short segment along the western edge, which coincide with the France – Belgium border. The domain covers an area of 422.3 km², discretized into 42 234 two-dimensional square 100×100 m cells. This regular spatial discretization constitutes a compromise between accuracy and processing time, for flow as well as for solute transport computation.

Vertically, 12 layers of cells with varying thickness are used to represent the whole geological sequence. The upper limit of the model corresponds to the ground surface, defined by a numerical terrain model. The lower limit of the model is set to the base the aquifer, corresponding to the bottom limit of the Cretaceous layers, as defined by Dupont (2021). The first three layers below the ground surface correspond to the alluvial deposits, the Ypresian sands and clays, and the Thanetian sands and clays. The top and base of these three layers are implemented based on Rorive and Van Wittenberge (2004). The nine cell layers located below represent the main cretaceous chalk aquifer. They are distributed vertically throughout the total aquifer thickness, with slightly thinner layers at the bottom. Due to the aquifer geometry, the number of active layers varies according to the total thickness of the aquifer, which differs greatly between the center of the basin (around 400 m) and the margins of the model where the chalk aquifer is much thinner (Figure *4*). This vertical discretization of the chalk aquifer pursues two goals. First, it allows for more precise adjustment of hydraulic conductivity both horizontally and vertically within the active domain during the calibration of the steady-state flow model. Second, it enables a more detailed vertical propagation of nitrate in the aquifer, as simulated by the solute transport component of the numerical model.

Figure *4* presents a three-dimensional view and a vertical cross-section of the model grid. These two views can be compared to the hydrogeological map and the geological cross-section shown in Figure *1*.

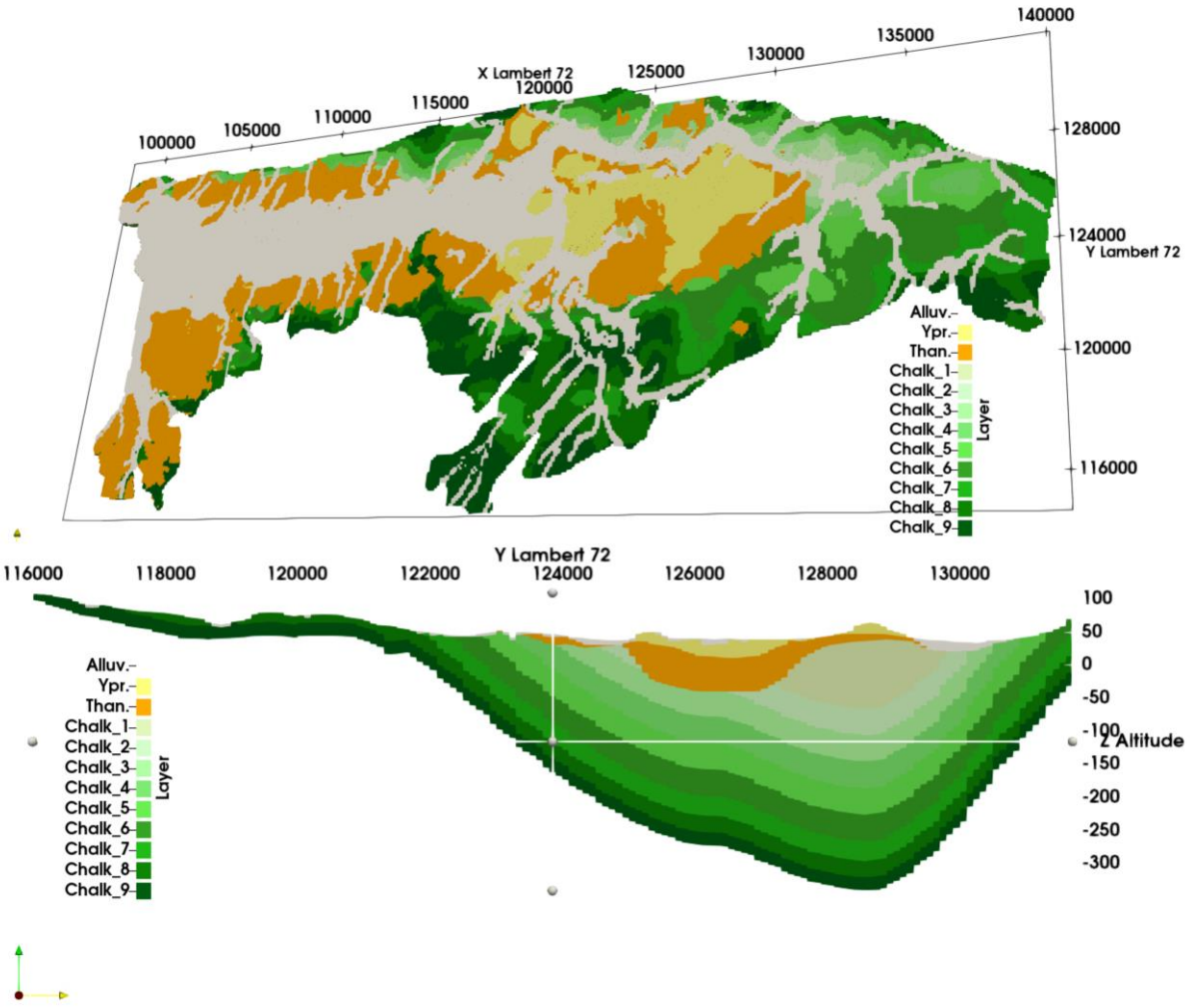

291

292 Figure 4: a) Three-dimensional view of the model grid b) Vertical cross-section of the model grid. Vertical distances (Z axis)
293 are exaggerated by a factor of 10 for visibility reasons. Alluv.: Alluvial deposits; Ypr.: Ypresian; Than.: Thanethian.

294 The flow model is developed under steady-state conditions. Five stresses and boundary conditions are
295 considered: (1) groundwater recharge, (2) abstraction volumes from water production wells, (3)
296 influence of the hydrographic network, (4) the physical limits of the aquifer, and (5) groundwater flow
297 leaving the modelled area through the western France - Belgium border.

298 Recharge is here considered homogeneous over the entire aquifer and is set at 170 mm/year, according
299 to the mean recharge volume estimated by Rorive (1983) and adapted to the actual modelled area.
300 Groundwater abstraction volumes from 2018 by the public water companies, the industries and private
301 wells are used as model inputs. Only the wells producing more than 6,500 m^3/year are included. Their
302 locations are shown in Figure 1c). All the pumping wells implemented in the model extract 44×10^6
303 m^3/year of groundwater, corresponding to 95% of the total volume abstracted in 2018. The multi-aquifer
304 well (MAW) package (Langevin et al., 2017b), which distributes the volumes withdrawn by each well
305 over several numerical layers according to hydraulic properties, is used in the developed model. In the
306 Mons Basin aquifer, wells are typically drilled within the upper chalk layers and do not generally reach
307 the less-productive marly chalk lower down in the sedimentary sequence. In the model, the less
308 productive chalk corresponds to numerical layers 9 to 12.

309 The hydrographic network implemented in the model consists mainly of the 'Haine' River and the most
310 important tributaries (Figure 1c). Based on the observations made in Rorive (1983), most of the streams
311 in the basin are considered as draining the aquifer, with no discharge from the surface to the subsurface

compartments. All rivers are therefore represented using the drain package (Langevin et al., 2017b). The drained cells are located along the main riverbeds at the highest cell of non-zero thickness encountered. They are mostly within the first model layer and associated with alluvial deposits.

According to the geological context, the low-permeability marl layer at the base of the aquifer allows imposing a no-flow Neuman boundary condition along almost all external limits of the model. The only exception is the western limit, which does not correspond to a physical border but to the political frontier between France and Belgium, in a flat marshy area, also constituting the outlet of the catchment. According to the 2015 piezometric map (Figure *1*a), groundwater fluxes are however mainly parallel to this limit, with groundwater flowing directly to the Haine River rather than across the border. The quantity of groundwater flowing directly to France from east to west is therefore limited. Along this limit, a Dirichlet constant head boundary condition is set at the level of the ground surface elevation on cell layers corresponding to the chalk aquifer beneath the alluvial plain (Figure *1*(c)). Consequently, a small quantity of groundwater flows through this specific boundary condition, from the Belgian part of the chalk aquifer to France.

3.2. Transport model stresses

For the transient solute transport model, the applied stresses include nitrate inputs from diffuse agricultural nitrogen percolation and potential leakage of contaminated water from the sewer system. The advection – dispersion transport equation is solved implicitly with a full upstream scheme. Boundaries for solute transport are implemented as Neumann conditions, implying no dispersion flux. As a result, nitrate can exit the model domain by advection through pumping wells, rivers and the western model boundary.

Diffuse nitrate input data from agricultural sources are derived from the results of the EPIC Grid model described by Sohier and Degre (2010). This model is a spatial generalization of the EPIC ("Erosion-Productivity Impact Calculator") model (Williams and Singh, 1995), applied to Wallonia (Belgium) and adapted to the region's soils, land use, climate, and agricultural practices. This mixing model simulates the nitrogen cycle and all related transformations (including mineralization and reorganization) based on agricultural practices and weather conditions. It covers the portion of soil from the root zone to the top of the fully saturated zone and therefore provides estimates of the amount of nitrogen percolating down to the water table. These estimates are used as an input for the solute transport component of the groundwater model. The input data used consist in transient mass fluxes expressed in kilograms of nitrogen per hectare (ha) per day (1 ha = 10^4 m^2). It is assumed that all percolating nitrogen is fully converted to nitrate. The time resolution of the input data is daily. Regarding spatial discretization, these input nitrate mass fluxes correspond to square cells of 1 km^2. Consequently, each EPIC Grid cell corresponds to 100 cells in the MODFLOW model.

Figure *5* illustrates the spatial and temporal variations of input data provided by the EPIC Grid model across the study area. Three different periods are visible in the time series. The data shown in blue correspond to the values calculated by the EPIC GRID model for the period 1971-2022, based on historical agricultural practices and meteorological data. These "historical" inputs are used to calibrate the solute transport model according to the observed nitrate concentrations. Data in black, from 1950 to 1970, correspond to a model warm-up phase. As nitrogen input data prior to 1970 are not known or simulated, a linear increase in nitrogen mass inputs was generated, as an estimation of the nitrate mass fluxes in the aquifer prior to 1970. The only purpose of this pre-1970 phase is to limit the impact of the initial concentration set in each cell at the start of the simulations. Data in green show an example of future nitrogen inputs simulated by the EPIC Grid model, based on different climate and farming practices scenarios for the period 2023-2050. This aspect is discussed more extensively in the ***Modelling of future nitrate concentrations*** section.

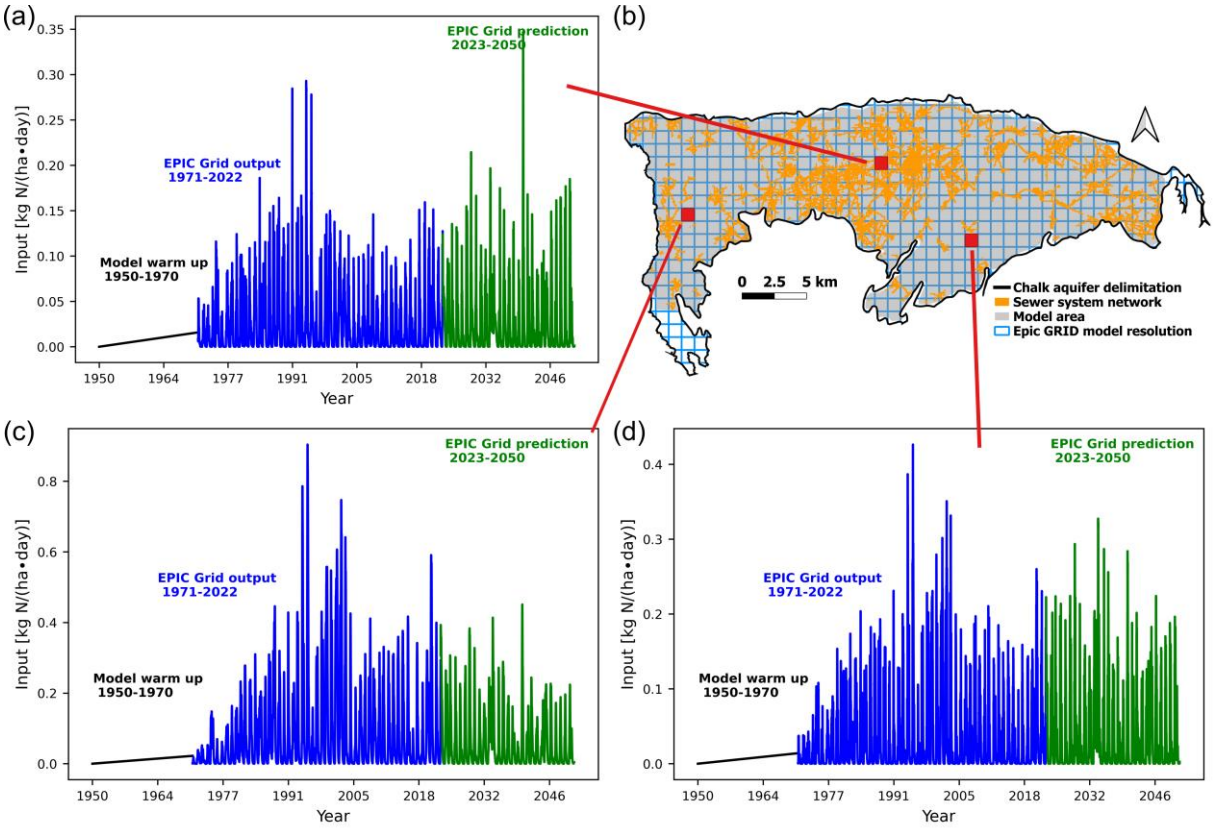

Figure 5: a), c) and d) Examples of three agricultural nitrogen diffuse infiltration timeseries, from 1950 to 2050 with a daily time step discretization. Each time series is associated to a different 1 × 1 km² area and masses are expressed in kilograms of nitrogen per day per hectare. From 1950 to 1970, the black line corresponds to the assumed nitrogen input during a "warm-up phase" of the simulation. From 1971 to 2022, the blue line corresponds to the historical amount of infiltrating nitrogen calculated by the EPIC Grid model (Sohier et al., 2009; Sohier and Degre, 2010). From 2023 to 2050, the green line corresponds to one of the outputs of the EPIC Grid model, when simulating a specific scenario of climate and agricultural practice. In this figure, it corresponds to a climate change with temperature rise qualified as medium ('MARm') and farming practices similar to the current situation ('Tend'). (Sohier and Degre, 2016) This aspect is further described and discussed in the ***EPIC 2023 – 2050*** section. b) Map of the model area showing the spatial discretization of the EPIC Grid model (blue grid). The groundwater model cells (100×100 m²) where a contamination associated to sewer leakage is simulated are shown in orange.

The sampling campaigns described in Christiaens et al. (2023) highlighted a of contamination of the aquifer by leakage from the wastewater sewage system in urbanized areas. Although the location of the sewer network is well identified, the position of potential leaks remains unknown. Therefore, to simulate the overall impact of this pollution source on nitrate concentrations, a uniform percentage of wastewater loss is applied as a mass input to all cells where a sewerage system is present. The value of this mass input is derived from the volumes of wastewater treated by the wastewater treatment plants present in the studied area (22×10^6 m^3) and the average nitrogen concentration in this water (48.125 mg N/L) in 2017. The results presented here assume a 10% loss rate, corresponding to a nitrate mass input of 27.62 g N/(ha·day) in the concerned cells (shown in orange in Figure 5b)).

3.3. Parameterization

For each parameter, a constant value is assigned to all cells within each layer. Consequently, a given parameter can have a maximum of 12 different values. This approach maintains a certain degree of horizontal and vertical heterogeneity in the model, consistent with the geometry of the geological units.

Since the flow equation is solved under steady-state conditions, the only parameter defined for the flow component is the hydraulic conductivity (K, in m/s) which is assumed to be isotropic. Different K values

are assigned for the layers corresponding to the alluvial deposits, the Ypresian and Thanetian sands and clays, and the nine layers of cells representing the Cretaceous chalk aquifer.

Regarding the solute transport component of the model, several parameters are considered. Given the chalky nature of the aquifer, a dual-porosity system is implemented. Although the total porosity of the chalk matrix is usually high, the effective drainage porosity, mainly explained by the presence of fractures, is generally much lower. To account for this reality in the model, three parameters are implemented: mobile porosity, immobile porosity and a transfer coefficient between both of them. For mobile porosity, four different values are assigned to the four main lithologies (alluvial deposits, Ypresian sands/clay, Thanetian Sands/clay and chalk aquifer). A uniform value is assigned to all cell layers corresponding to the chalk aquifer. Immobile porosity is neglected in the upper three layers (Cenozoic deposits), as they are predominantly composed of sand, and despite containing thin layers of clay. This type of sandy lithology actually generally presents low values of immobile porosity compared with total porosity (Dassargues, 2018). Sensitivity analysis confirmed better results when immobile porosity was neglected in these three layers. In the underlying main aquifer, despite the heterogeneity between the different geological units (limestone, tuffeau, white chalk, marly chalk), the immobile porosity and mobile/immobile transfer coefficient are considered as constant across layers 4 to 12. Finally, uniform values of longitudinal and transverse dispersivity are implemented for all cells. These simplifications were adopted in absence of clear information regarding the heterogeneity of those parameters in the chalk aquifer. They also serve to keep the model as simple as possible and to minimize the risk of introducing errors associated with potentially unrealistic conceptual assumptions. Due to the predominantly diffuse nature of the nitrate sources and the horizontal dimension of the cells (100 m × 100 m), the contribution from mechanical dispersion may be low, compared to the spreading of fertilizers and numerical dispersion linked to cell size. Despite sensitivity to dispersivity parameters is low, they contribute nonetheless to improve the model performance during calibration.

3.4. Calibration

The model parameters are calibrated on a trial-and-error basis by comparing: (1) observed and simulated piezometric levels, as well as the inflow and outflow water balance terms under steady-state conditions; (2) observed and simulated nitrate concentrations using data from previous sampling campaigns (Christiaens et al., 2023), complemented by additional data provided by water producers.

3.4.1. Calibration of the model flow component

Calibration of the groundwater flow-related hydraulic parameters is guided by prior knowledge and data. (1) The general geological and hydrogeological understanding of the Mons Sedimentary Basin is essential, including the observed decrease in hydraulic conductivity with depth as the chalk becomes more marly. Due to the geometry of the aquifer, transmissivities are generally higher in the center of the basin, where the aquifer is thicker, compared to areas where older deposits outcrop. (2) The hydrogeological maps of the region (Mengeot et al., 2017a) gives valuable information on hydraulic conductivity trends in the chalk layer. (3) Values used and calibrated in previous models (ex. Rorive and Van Wittenberge, 2004) provide references for the hydraulic conductivities of the four main hydrogeological units (alluvial, Ypresian, Thanetian and cretaceous chalk deposits).

The values of hydraulic conductivity assigned to each numerical layer after calibration are presented in Table *1*. They are consistent with the general knowledge and data exposed previously.

Table 1: Calibrated hydraulic conductivity values for each layer of cells.

Numerical layer	Lithology	Hydraulic Conductivity (m/s)
1	Alluvial	0.00025
2	Ypresian sand/clay	0.000005
3	Thanetian sand/clay	0.00002
4	Chalk	0.0001
5	Chalk	0.000075
6	Chalk	0.000075
7	Chalk	0.00005
8	Chalk	0.00005
9	Chalk	0.00005
10	Chalk	0.00005
11	Chalk	0.00003
12	Chalk	0.0000075

Table *2* shows the balance between the model's input and output flows. Recharge and groundwater abstraction are prescribed stresses in the model. At equilibrium, the recharge amounts to 69.7×10^6 m³/year across the entire modelled area. This value is 3% lower than that imposed in the recharge package (see the ***Mesh and flow conceptual modelling*** section), due to the drying out of some thin zones, close to the limits of the model, during convergence. This is consistent with field observations, where the marly, less permeable chalk at the basin edges plays a minimal role in aquifer storage. Production wells constitute the largest simulated outflow, accounting for 63% of the recharge. The second most important outflow is the exfiltration to the river system, representing about 32% of recharge. As expected and suggested by the piezometric map (Figure *1*), only a relatively small volume of groundwater exits the model domain through the western boundary condition. The overall simulated water balance is considered accurate and unbiased (error: -0.045%) and corresponds to the current hydrogeological understanding of the aquifer.

Table 2: Overall water budget for the calibrated steady-state model. Positive values correspond to inflows to the model, whereas negative values indicate outflows.

Water budget component	m³/year	% of recharge
Recharge	69.7×10^6	100.0
River network drains	-22.6×10^6	-32.4
Water production wells	-44.1×10^6	-63.2
Constant head west boundary	-3.7×10^6	-4.4
Error	-0.03×10^6	-0.045

Figure *6* illustrates the relationship between the observed and the simulated piezometric levels. The dataset compiles mean piezometric levels calculated from various data sources and campaign conducted between 2000 and 2023. A total of 114 reference piezometric points were used in the calibration process. The blue dots represent simulated values within a ±5 m range of the observed values. These points are located throughout the modelled area. Some overestimations of piezometric levels (red dots – *i.e.* more than 5 m) are consistently observed in the southeastern part of the aquifer. This is most likely due to the simplification of the hydrographic network, which artificially restricts outflows to rivers. In this part of the aquifer, the thinner, marly chalk layer facilitates direct flow or runoff towards small natural streams, which are not fully represented in the model. Despite this, given the scale of the model, the regional

piezometric trends, and the observed seasonal variations, this steady-state calibration is considered as very good and is used for the solute transport component of the model.

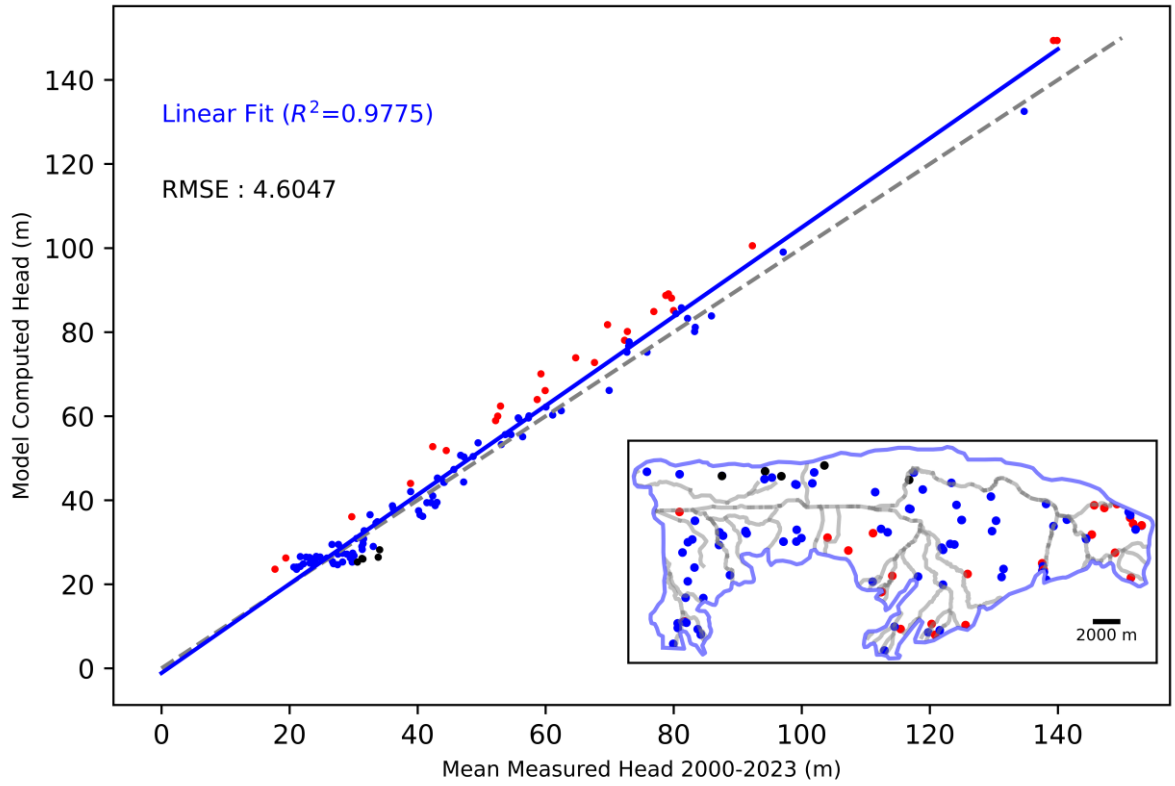

Figure 6: Comparison of observed and simulated piezometric levels. Red dots correspond to observed levels overestimated by more than 5 m. Black dots show levels underestimated by more than 5 m. Blue dots correspond to simulated levels within an interval of 5 m around the observed value. The blue line corresponds to a linear regression on all points (blue, black, red - R^2 = 0.9775). The grey dashed line corresponds to a perfect match (1:1) between field measurements and calculated piezometric levels. RMSE: root-mean-square error.

3.4.2. Calibration of the model solute transport component

The regional scale of the model makes the determination of transport parameters a complex task. Estimates based on local tracer tests are available in the regional hydrogeological maps (Mengeot et al., 2017a), but these parameters are generally scale and experiment-dependent, and extrapolating them to a larger scale introduces uncertainty. In this study, transport parameters are calibrated based on observed nitrate concentrations in groundwater, while keeping values within typical ranges for the studied lithologies (Dassargues, 2018). The calibration process is supported by a sensitivity analysis, performed on transport parameters and stresses with respect to simulated concentrations, which provides insight into the most influential parameters on the simulated results. Variations in simulated concentrations at specific points (first chalk numerical layer at the end of 2022), when the value of a parameter or an input stress is modified by one percent, are assessed. The sum of the variations weighted by the relative variation of the parameter or stress, squared and divided by the number of observation points (see Eq.1) is used as an indicator of nitrate concentration sensitivity. Results of this sensitivity analysis are presented in Figure *7*. These sensitivities correspond here to the calibrated values of the transport parameters shown in Table 3.

$$\sum_{i=0}^{ND}\left(\frac{\left[\left(y_i(b+\Delta b)-y_i(b)\right)\times\left(\frac{b}{\Delta b}\right)\right]^2}{ND}\right) \quad \text{Eq.1}$$

Where:

$y_i(b)$: simulated nitrate concentration at point i with the set of parameter and stress values b

$y_i(b+\Delta b)$: simulated nitrate concentration at point i with the set of parameter and stress values b modified by Δb. In this study, parameters or stress values are modified individually.

$\frac{b}{\Delta b}$: Ratio between the absolute default value of the parameter and its absolute modification

ND : The total number of observation points

Investigated parameters include the mobile and immobile porosities, the transversal and longitudinal dispersivities, as well as values associated with initial conditions. Stresses include the quantity of diffuse agricultural inputs and the contamination from the sewer network. The analysis reveals that the highest sensitivities are clearly related to the input stresses, highlighting the potential impact of uncertainties linked to these inputs. In third and fourth position, the value of immobile porosity in the chalk and the initial concentration set in the model have the most significant influence on the simulated results.

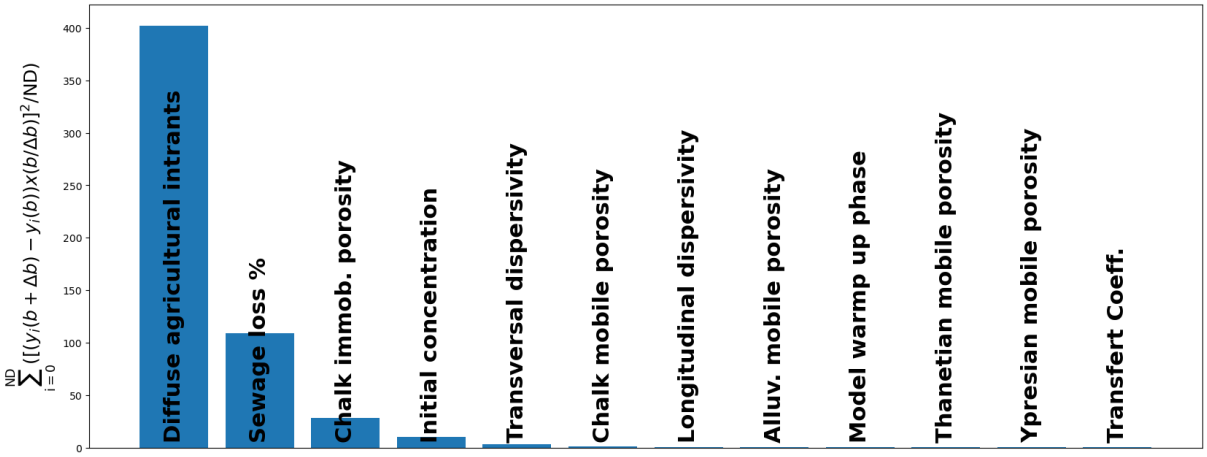

Figure 7: Sensitivity of the simulated nitrate concentrations against transport related parameters and stresses. The corresponding values of the transport parameters are shown in Table 3.

Regarding the parameter values assigned to the transport model after calibration (Table 3), mobile porosity ranges from 15% for alluvium, 5% for sandy-clay layers to 1% for chalk layers while the immobile porosity is set to a lower-than-expected value of 5%. The longitudinal and transversal dispersivity values are set to 100 m (the length of a model cell) and 10 m, respectively, for all layers. The value of the mobile-immobile transfer coefficient, associated here with a low sensitivity, has been defined based on the results of Orban et al. (2010) , focused on another cretaceous chalk aquifer in Belgium.

Table 3: Calibrated values associated to the solute transport parameters, by layers.

Numerical layer	Lithology	Mobile porosity (-)	Immobile porosity (-)	Longitudinal dispersivity (m)	Transversal dispersivity (m)	Mobile / Immobile transfer coefficient (-)
1	Alluvial	0.15	/	100	10	/
2	Ypresian sand/clay	0.05	/	100	10	/
3	Thanetian sand/clay	0.05	/	100	10	/
4	Chalk	0.01	0.05	100	10	0.0000001
5	Chalk	0.01	0.05	100	10	0.0000001
6	Chalk	0.01	0.05	100	10	0.0000001
7	Chalk	0.01	0.05	100	10	0.0000001
8	Chalk	0.01	0.05	100	10	0.0000001
9	Chalk	0.01	0.05	100	10	0.0000001
10	Chalk	0.01	0.05	100	10	0.0000001
11	Chalk	0.01	0.05	100	10	0.0000001
12	Chalk	0.01	0.05	100	10	0.0000001

Simulated nitrate concentrations are first compared to the corresponding concentrations measured during the 2020 and 2021 campaigns performed by Christiaens et al. (2023) (see Figure *3* and Figure *8*a, b and c). The quality of the calibration varies according to the groups, as further discussed below. Overall, however, simulated concentrations at the time of the 2020 and 2021 sampling campaigns are included between 9.73 and 51.74 mg/l with an average of 29.32 mg/l. These rather low values demonstrate the difficulty of the model in reproducing concentration peaks observed in samples collected in the field. This discrepancy between the simulation and the laboratory measurements is probably directly linked to the regional scale of the model and the size of the cells (0.01 km²), which tends to average out the simulated concentrations. Furthermore, for both the diffuse agricultural sources and wastewater contamination, the solute inputs incorporated into the transport component of the model are also already spatially averaged and homogenized at a resolution of 1 km × 1 km blocks for the EPIC Grid simulations, and at the scale of the sewer network, respectively. As a result, it can reasonably be expected that the model will not be locally faithful to all observed data, which may be impacted by very local sources of nitrate, which are averaged at a higher scale in the model inputs. The calibration, both overall and for each specific group, should therefore be interpreted globally rather than point-by-point, keeping in mind the spatial resolutions applied. These aspects are further discussed in the ***Discussion*** section.

Regarding the different groups highlighted by Christiaens et al. (2023), the graphs of Figure 8 show that Group B, characterized by a nitrate signature of mineral fertilizers origin, is the best represented by the model. The highest observed concentrations of Group A (manure signature) and Group C (mixed signature) are underestimated. While manure spreading is taken into account in the EPIC Grid inputs, more localized sources, such as manure stockpiles, are not represented in the model. These unrepresented sources could, in some areas, significantly increase the nitrate inputs and explain the underestimation. Conversely, observed concentrations of Group C (sewage signature) are slightly overestimated by the model, probably due to the simplistic assumption of a uniform 10% leaching rate all along the wastewater network. Finally, as expected, concentrations for piezometers located in confined zones, where active denitrification processes occur, are clearly overestimated. In its current state, the model does not include degradation and therefore overestimates concentrations in areas where denitrification actually reduces nitrate.

The availability of long-term historical concentration time series remains unfortunately limited. Figure *8*(d) compares the evolution of simulated and observed nitrate concentrations over time at four production wells between 1990 and 2020. The results demonstrate the model's ability to reproduce consistent concentration values in the upper numerical layers. Although the amplitude of simulated variations is generally lower, the order of magnitude and overall trends of simulated concentrations correspond to field measurements. The quality of the fit between observed and simulated data is generally acceptable but varies significantly depending on the location. For instance, as shown in Figure 8, concentrations at well 68, for example, is clearly underestimated.

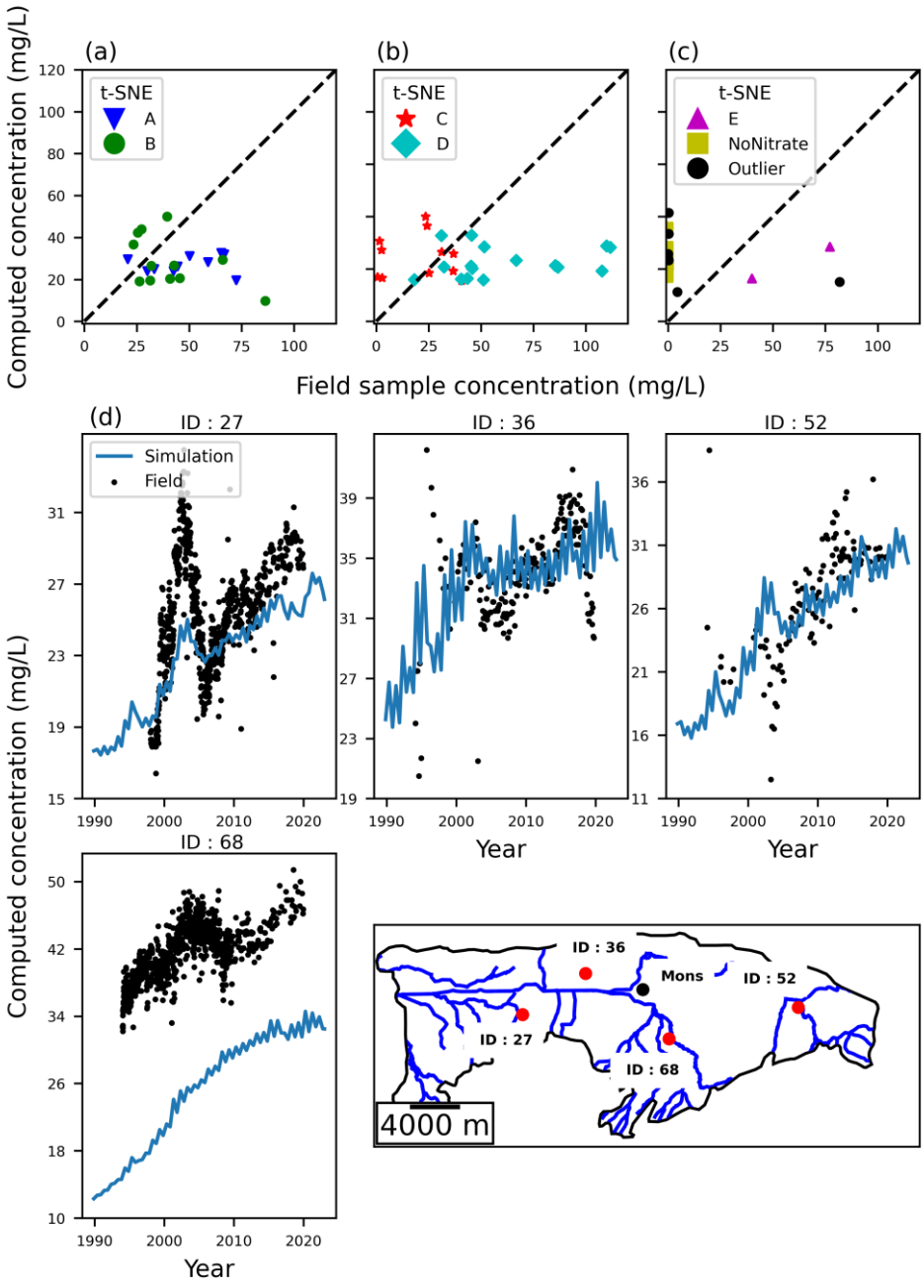

Figure 8: Comparison between simulated and observed nitrate concentrations. (a) (b) and (c): comparison between simulated and observed nitrate concentrations corresponding to sampling campaigns performed in 2020 and 2021. The samples are shown according to the statistical groups derived from t-SNE dimensional reduction, described in Christiaens et al. (2023) and associated with isotope signatures characteristic of different anthropological sources of nitrate (see also Figure 3). Group A: 'manure' signature; Group B: 'mineral fertilizer' signature; Group C: 'sewage' signature, Group D: 'mixed' signature. Group E does not present a clear signature and contains sampling points impacted by local pollution. (d): comparison between simulated and observed nitrate concentrations over time at four production wells.

4. Modelling of future nitrate concentrations

4.1.EPIC 2023 – 2050

Six predictive scenarios of agricultural nitrate input to the aquifer are applied to the model. These are derived from the results provided by the EPIC Grid model for the period 2023-2050 (Sohier and Degre, 2021, 2016). The objective is to simulate possible trends in nitrate concentration over the next thirty years. The six input scenarios result from combining two farming practice scenarios with three climate scenarios.

The first agricultural practice scenario is a “tendency” or "business as usual" scenario (abbreviated to "tend"), which assumes that farming practices will remain or evolve similar compared to the current situation. Its counterpart is a transitional scenario (abbreviated to "tran") for which the EPIC Grid simulation considers changes in agricultural practices in terms of land use, mineral fertilizer usage and the crop type. These two scenarios of agricultural practices were developed by Baret et al. (2019). For the “tend” scenario, the average trends (evolution of the percentage of land dedicated to agriculture, distribution between crop and livestock types) over the period 2005-2015 are extended to 2050. This leads to a 16% reduction in the total area dedicated to agriculture activities. This reduction is mainly due to the gradual disappearance of grassland dedicated to cattle farming. In the “tran” scenario, the total surface area dedicated to agriculture is maintained until 2050, with a strong emphasis on extensive livestock farming and the development of organic farming methods. Although initially designed with a focus on the use of pesticides, leading to a sharp reduction of 44%, this scenario is also used in the present study test to assess the impact on these changes on nitrate concentrations.

The three climate scenarios applied to the EPIC grid model are derived from the CMIP6 (Coupled Model Intercomparison Project Phase 6, (O’Neill et al., 2016). Regional climate projections are then calculated using the MAR atmospheric model (Modèle atmosphérique régional, in French). Initially developed for polar regions (Fettweis et al. (2013), this regional climate model was later adapted and applied to the Walloon region by Wyard et al. (2017). The three scenarios, referred as ‘MARc’ (cold), ‘MARm’ (medium) and ‘MARw’ (warm), are obtained by forcing the MAR model with global climate projections corresponding to different levels of warming. This ’warm’, ’cold’ and ’medium’ classification relies on the temperature increases expected for the 2080-2100 period. Of course, for nearer-term periods, the differences between the three scenarios may be less pronounced, and interannual variations in temperature and precipitation may temporarily diverge from the long-term trend defined by the 2080-2100 horizon.

Based on the agricultural practices considered and the outputs of the regional climate model, EPIC Grid recalculates time series of recharge values and nitrate fluxes, considering weather conditions, land use, plant growth processes and nitrogen volatilization, nitrification, denitrification and assimilation. By comparing mean recharge values for the 2000-2019 period to those calculated for each scenario (2031-2050), the MARw and MARc lead to recharge decreases of -3% and -7%, respectively. In contrast, the MARm scenario induces a 1% recharge increase over the same period. An example of the projected evolution of mass nitrate fluxes until 2050 is shown in Figure *5* for selected illustrative locations, under the ‘MARm’ climate scenario combined with the ‘tend’ agricultural practice scenario. The resulting evolution varies spatially, with globally decreasing or increasing trends depending on the location and context. In the groundwater model, these variations are implemented as changes in mass nitrate input fluxes.

Figure *9* shows the nitrate concentrations calculated by the MODFLOW 6 transport model at 3 production wells, based on these six combined scenarios. The concentration shown corresponds to the

top-most cell of the well in the chalk aquifer. From 2013 to 2022, all scenarios logically produce identical results, before diverging during the 2023-2050 period. At all observation points, simulated nitrate concentration generally remains stable or increases with time. This behavior directly reflects the EPIC Grid model outputs, which predict a global increase in nitrogen fluxes to groundwater across all scenarios, with significant impact of both climate change and changes in agricultural practices. To better highlight long-term trends that may be partly hidden by seasonal variations in Figure 9, average concentrations over the 2045-2050 period are shown as horizontal lines at the end of each curve. The MARm business-as-usual ('tend') and MARw transitional ('tran') scenarios consistently produce the most extreme outcomes. Among those six specific simulations, the influence of climate change appears significantly greater than the impact related to adaptations in agricultural practices. However, the number of tested scenarios here remains limited. This point is further discussed in the ***Discussion*** section 5.

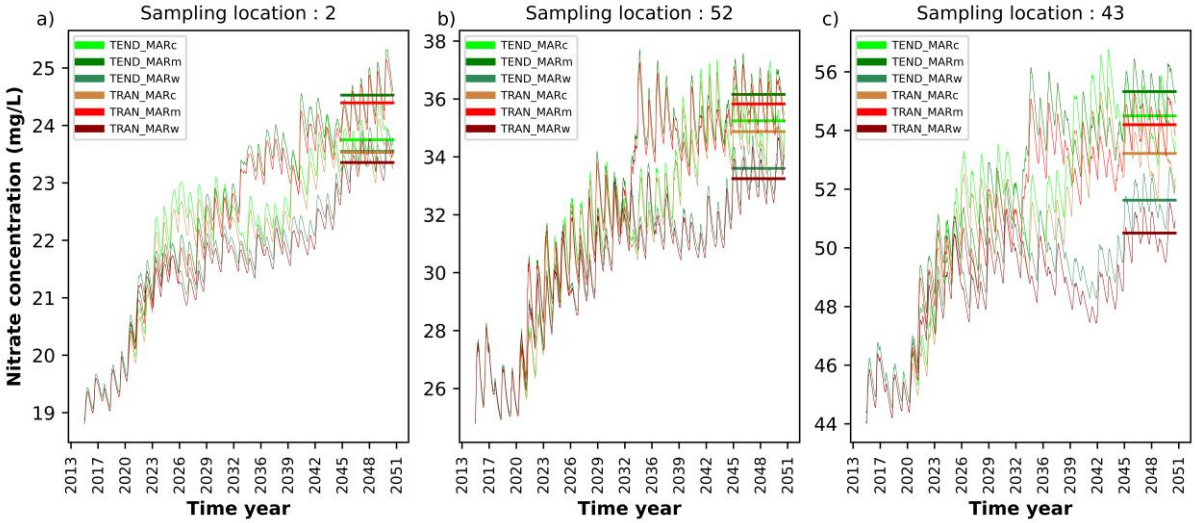

Figure 9: a), b) and c) Nitrate concentration computed at three different observation points, from 2013 to 2050. Each color corresponds to the response obtained from a different agricultural input predictive scenario. The black section up to 2022 corresponds to the end of period covered by similar input scenarios. Each horizontal line corresponds to the mean nitrate concentration computed over 2045-2050 for one scenario.

4.2. Sewage impact

Two predictive scenarios are simulated to assess the potential impact of sewage systems. They are both based on the diffuse agricultural input scenario combining historical nitrate fluxes before 2023 and the scenario "MARm - tend" (described in the ***EPIC 2023 – 2050*** section), covering the period from 2023 to 2050, as provided by the EPIC Grid model. These agricultural inputs are here combined with a contamination of the aquifer by the sewage system. In the first scenario (represented by the blue line in Figure 10), sewage contamination remains constant and continuous throughout the entire simulation period (see the ***Transport model stresses*** section). In the second scenario (represented by the red line in Figure 10), sewage contamination follows a similar pattern but ceases entirely after 2025. From this point, the sewers are assumed to be watertight, with only agricultural nitrate inputs considered in the model.

Figure *10* shows the nitrate concentrations simulated by the model at three wells from 2010 to 2050. Depending on their location relative to the sewage system, wells react differently to variations in inputs.

The ID 36 well, for example, is located relatively far from urbanized areas. The difference in concentration, whether there is leakage from the sewer network or not, is not significant there and it is mainly agricultural inputs that explain the simulated nitrate contamination of the well. This conclusion

does not fully align with the analyses described in Christiaens et al. (2023). On the basis of isotopic analyses, this area actually appeared to be affected by contamination from wastewater. This discrepancy between field interpretations and simulations can be explained by the large presence of unconnected wastewater disposal pits reported by local residents to public services (IDEA, 2015). As this type of local source is not represented in the model, the simulation does not reflect their contribution to the total nitrate concentration. Conversely, the other two wells of Figure *10* are located in the center of a more urbanized area. Stopping the sewage contamination from 2025 leads to a much higher decrease in nitrate concentration compared to the default scenario. In these locations repairing the sewage system would significantly contribute to reducing the nitrate pollution after 2025.

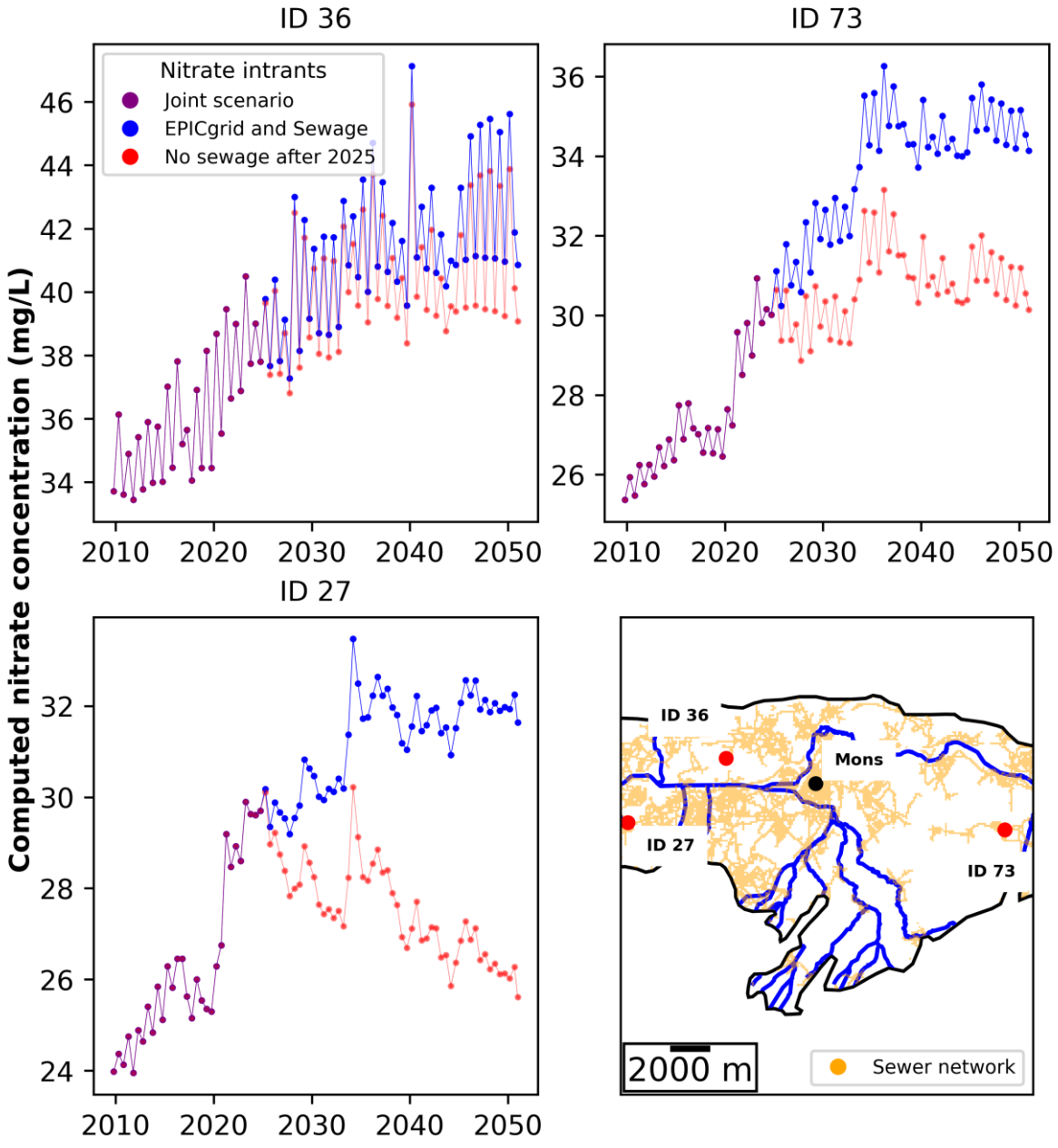

Figure 10: Nitrate concentration simulated from 2010 to 2050 at three different locations. Two different nitrate input scenarios are considered. In blue, a predictive scenario of agricultural inputs is coupled with a continuous and constant contamination of the aquifer by the sewer system. In red, the same predictive scenario of agricultural nitrate inputs is considered but the contamination of the aquifer by the sewer network is fully stopped from 2025 until the end of the simulation. Simulated data in purple are common for both scenarios.

5. Discussion

After development and calibration, the model is used to represent long-term trends in nitrate concentrations in the aquifer, considering pollution inputs of agricultural and sewage origins. It is efficiently combined with predictive input scenarios to provide future trends of pollution levels at the scale of the whole groundwater body. Before concluding on the projected impacts, several aspects and limitations of the methodology used are discussed below.

Despite the integration of a diffuse agricultural input and the assumption of a specific contribution from the sewage system, comparison of simulated results with measured values still reveals that the model generally underestimates calculated concentrations, in particular for some of the specific groups identified by Christiaens et al. (2023) (see also the ***Calibration of the model solute transport component*** section). There are multiple possible reasons for explaining this discrepancy.

The sensitivity analysis presented in the ***Calibration of the model solute transport component*** section demonstrates the crucial influence of the prescribed nitrate inputs on the concentrations simulated in the aquifer. While calibration, particularly of transport parameters, could be improved by further model development or investigations (e.g. values of porosities, vertical discretization), the reliability of the data used as inputs primarily influence simulated values and how they fit with those measured in the field. Those input data are therefore of particular importance.

Regarding agricultural inputs, even if they are spatially distributed, they remain affected by a certain degree of homogenization at the scale of 1 km × 1 km blocks, which may contribute to artificially smooth out local heterogeneities and related concentration peaks. The EPIC Grid model was originally developed at the scale of the whole Walloon region (~17 000 km²), and not at the scale of each aquifer or groundwater body. Second, the EPIC Grid simulations do not incorporate the contribution of local sources of nitrogen. The many manure dumps deposited over the area, the organic matter contained in landfills or specific industrial sites, for example, can concentrate a large quantity of nitrogen, generate additional local pollution, and surely contribute to the general contamination of some aquifer areas.

Still about the nitrate inputs into the groundwater compartment, the way the pollution from the sewer network is incorporated into the model is imperfect, due to the lack of detailed data on volume of leakage, nitrogen load, and precise leak locations. The contribution from the sewer network is currently represented as constant over time and uniformly distributed across all model cells intersected by the sewer network. In reality, the pollution is likely concentrated in more localized "hotspots", probably in the oldest sections of the infrastructure. This simplifying assumption may thus easily lead to local over- or underestimation of simulated concentrations. Despite these simplifications, the model is however proved useful in different ways in terms of understanding the contamination of the aquifer by sewage.

Finally, the groundwater model has been developed at a large scale, crucial for studying global trends, considering diffuse nitrate sources. The spatial resolutions (100 m ×100 m horizontally and thickness ranging from 2 to 120 m with a mean thickness value of 13 m), as well as the simplifications needed for modelling at this scale may also smooth concentrations and explain discrepancies between simulated and observed values. Wells screened levels, for example, may be inaccurate and generally longer in the groundwater model, contributing to decrease simulated concentration for collected samples representative of more superficial groundwater.

In this context, as previously mentioned, the quality of the calibration should be evaluated globally, rather than drawing conclusions for individual observation points. Furthermore, grouping observations points based on the sources of nitrate, following the approach of Christiaens et al. (2023), and assessing calibration performance separately for each group, is recommended and contribute to make the process

more transparent and relevant. We consider that integrating these groups into the calibration process constitutes an interesting contribution, as illustrated in this study.

The spatial resolution of both nitrate inputs and groundwater model is an important aspect of the problem, as previously discussed. Refining the grids may allow a better representation of local pollution sources and enhance the accuracy of simulated plume propagation. In this exercise, the mesh structure and the capabilities of MODFLOW 6 offer valuable flexibility. The grid can be locally refined where needed, allowing the model to focus on localized issues within the aquifer.

In this study, MODFLOW6 and EPIC Grid simulations are efficiently combined. While the approach meets the initial needs, the way the problem is conceptualized also presents some limitations. The EPIC Grid model is developed under transient conditions, and therefore accounts for seasonal dynamics, weather variability and the timing of agricultural operations. It simulates daily variations in water and nitrate fluxes within the soil and partially saturated zones. These variable nitrate mass fluxes are then prescribed as input of the MODFLOW6 model, at the top of the fully saturated zone. Although the solute transport component of this MODFLOW model is also transient, the groundwater flow component is implemented in steady-state conditions. Simulated groundwater flow in the saturated zone thus remains constant over time, possibly simplifying or averaging seasonal variations in dilution and flow velocities. Nevertheless, the nitrate mass balance is here fully preserved. Daily transient nitrate mass fluxes are calculated by EPIC Grid in the partially saturated zone, considering weather and recharge variations across time. These daily transient nitrate mass fluxes, rather than the related concentrations, are used as inputs to the MODFLOW solute transport model. This ensures that seasonal and short-term nitrate mass balance is respected, what is of course crucial, even if the groundwater flow in the fully saturated zone is permanent. This remains a simplification, which must be evaluated in light of the hydrogeological context. In the chalk aquifer of the Mons Basin, this impact may be limited, as observed seasonal and interannual groundwater head variations generally remain within a few meters, and the projected changes in annual recharge under the climate scenarios are expected to change by a few percent only (-7, +1 and -3% - see the ***EPIC 2023 – 2050*** section). If necessary, the steady-state flow model could be extended to transient regime using MODFLOW6, which is perfectly suited to such development. It would however induce a significant increase in computational time and substantial effort in calibration, to avoid amplifying the uncertainty with the model complexity. A full integration of the EPIC Grid and MODFLOW models would also require feedback mechanisms regarding simulated groundwater heads at each step.

The model does not account for any solute degradation processes within the aquifer. According to available data and Christiaens et al. (2023), it is clear that a variety of hydrochemical conditions leads to significant spontaneous denitrification, which reduces or completely removes nitrate in certain areas. In the studied chalk aquifer, denitrification varies with depth, lithological characteristics, and the presence of overlying confining layers. It is primarily observed in the central part of the basin, beneath alluvial deposits. Given the complexity of the processes, the challenges in representing them numerically, and the current lack of data on in-situ degradation rates, denitrification is currently not represented in the model. As a result, unrealistic nitrate concentrations are simulated in the specific areas where active denitrification occurs. Predictions made with the current version of the model therefore focus primarily on the unconfined zones of the aquifer, where elevated nitrate concentrations remain a persistent and critical concern for the environment and drinking water production. Simulations also provide information about the distribution and evolution of nitrogen concentrations at the interface, with confined zones. Nonetheless, incorporating denitrification processes into future versions of the models remains a significant area for further development.

Six projected scenarios have been used to investigate the influence of climate change and agricultural practices. While the results offer interesting insights regarding the potential impacts, this number of scenarios remains limited and does not provide an exhaustive overview. For example, the two agricultural scenarios (“tend” and “tran”) only concern four agricultural sectors in Wallonia (cattle

742 farming, cereal crops, potatoes and beets growing). The agricultural transitional scenario ("tran") was
743 primarily based on a change in the proportions between organic and traditional farming methods, as well
744 as in the extent of land devoted to cattle, rather than being specifically designed to address nitrate-related
745 issues. Therefore, the transitional scenario ("tran") does not have a drastic impact on the quantities of
746 nitrogen needed to support agricultural production. Consequently, other, more radical, scenarios,
747 questioning the distribution of surface areas dedicated to each type of crop, could result in more
748 significant differences in the quantities of fertilizers used. Similarly, just a few climate change scenarios
749 are considered in this study. Although it was not the primary objective here, increasing their number and
750 diversity would give a more comprehensive picture of the projected climate change impact on nitrate
751 spreading in the aquifer.

752

753 # 6. Conclusions

754

755 The groundwater model MODFLOW 6 and the agronomic model EPIC Grid have been used to
756 simulate groundwater flow and nitrate transport in the chalk aquifer of the Mons sedimentary Basin,
757 considering different sources as suggested by the isotopic analyses described by Christiaens et al. (2023).
758 MODFLOW6 allowed implementing and using a complex multi-layer numerical grid, which is more
759 adapted to the specific geology of the Mons sedimentary Basin, compared to previous versions of the
760 famous calculation code. To our knowledge, the model presented in this paper is one of the first which
761 has been developed for nitrate transport in aquifer, at large scale, using MODFLOW 6. The groundwater
762 flow component of the model was calibrated in steady-state based on observed mean piezometric levels
763 covering the period 2000-2020. The solute transport component of the model, calibrated in transient
764 conditions to historical nitrate concentrations, is used to simulate long-term trends in nitrate
765 concentration in the chalk aquifer. In addition to more classical transport parameters, it also includes a
766 dual porosity scheme, in which a specific immobile transport porosity is assigned to the chalk aquifer
767 units. Simulations consider two types of nitrate source. (1) Diffuse inputs caused by excess agricultural
768 fertilizers (mineral fertilizers and manures) percolate down to the aquifer. The spatial distribution and
769 amplitude of this contamination is directly deduced from the EPIC Grid model simulations. Based on
770 crop types, fertilizer quantities and the meteorological conditions, EPIC Grid calculates the excess
771 nitrogen that reaches the aquifer. (2) Inputs caused by potential losses from the wastewater network are
772 also considered. They are calculated based on the layout of the network and the average quantities of
773 nitrogen present in the wastewater arriving in the treatment plants. The sensitivity analysis conducted
774 on the MODFLOW model highlights the predominant influence of the solute inputs on simulated nitrate
775 concentration, underlining the critical importance of a reliable and accurate quantification of the
776 considered nitrate sources.

777 Simulations cover a historical period from 1970 to 2022 and a predictive time slice up to 2050 for which
778 six different future diffuse agricultural input scenarios, provided by the EPIC Grid model, are simulated.
779 The results obtained using these predictive scenarios show that all the climate/agricultural scenarios
780 considered lead to an increase, or at least a stabilization, of current nitrate concentrations. Although the
781 magnitude of the variations differs according to the locations, a general increasing trend is simulated
782 throughout the aquifer and correspond to the conclusions set out by Sohier and Degre (2021, 2016) about
783 the EPIC Grid model. (1) An increase in nitrate concentrations is simulated regardless of the agronomic
784 scenario. The transitional scenario ('tran') leads to slightly lower concentrations than the business-as-
785 usual scenario ('tend'). (2) The greatest impact on the intensity of the nitrate contamination comes here
786 from the selected meteorological scenario rather than the modifications of agricultural practices. The
787 scenario with medium climate change (MARm) leads to the highest nitrate concentrations, compared to
788 the cold (MARc) and warm (MARw) scenarios. The number of scenarios remains however limited and
789 the overall range of simulations must be further expanded. In particular, scenarios involving more drastic

changes in agricultural production methods, targeting nitrate-related issues, must be explored with the aim of more effectively reducing nitrate concentrations in the aquifer.

The representation of contamination from the sewage network into the numerical model brings several insights. Results highlight the importance of taking sewage pollution into account to be able to realistically represent the nitrate concentrations observed in the most urbanized regions of the study area. Although some assumptions are here simple, results support the identification of the production wells most likely to be affected by wastewater pollution. This information can then be used to guide further investigations aimed at pinpointing possible leakages and wastewater flows escaping from the network.

Some aspects of this study could be further refined or complemented, as discussed in Section 5. Nevertheless, the approach and the results provide valuable insights which contribute that support ongoing research and policymaking related to nitrate management in groundwater resources. The methodology has been designed at the regional level, combining groundwater and agronomic models. It accounts for various diffuse nitrate sources, in the calibration process and simulations, also integrating the impact of agricultural practices and climate change. The methodology followed, using the new MODFLOW6 version, provides a flexible tool designed to accommodate further developments, including the addition of new inputs, new local sources (e.g. manure local deposits, industrial sources, landfills), grid refinement, higher-resolution parameterization, particularly for the transport component. It can be easily adapted to address more local issues, while benefiting from the regional-scale results, or to incorporate complimentary aspects such as contamination by other substances.

Acknowledgements

We thank the water production companies IDEA, SWDE, Vivaqua and Farys for sharing some data and making some facilities available in the framework of this project.

On behalf of all authors, the corresponding author states that there is no conflict of interest

Funding information

This research was financially supported by SPGE (Société Publique de Gestion de l'Eau – Public Water Management Company), which is a public limited company set up by the Walloon Region.

7. References

Abascal, E., Gómez-Coma, L., Ortiz, I., Ortiz, A., 2022. Global diagnosis of nitrate pollution in groundwater and review of removal technologies. Science of The Total Environment 810, 152233. https://doi.org/10.1016/j.scitotenv.2021.152233

Bakker, M., Post, V., Hughes, J.D., Langevin, C.D., White, J.T., Leaf, A.T., Paulinski, S.R., Bellino, J.C., Morway, E.D., Toews, M.W., Larsen, J.D., Fienen, M.N., Starn, J.J., Brakenhoff, D.A., Bonelli, W.P., 2023. FloPy v3.5.0.dev0 (preliminary): U.S. Geological Survey Software Release.

Bakker, M., Post, V., Langevin, C.D., Hughes, J.D., White, J.T., Starn, J., Fienen, M.N., 2016. Scripting MODFLOW model development using Python and FloPy. Groundwater 54, 733–739.

Baret, P., Antier, C., Petel, T., 2019. Quelles agricultures wallonnes aujourd'hui et en 2050 ? (Walloon Agriculture Today and in 2050?). https://sytra.be/fr/publication/agricultures-wallonnes-2050/

Bastien, J., Roland, S., Rorive, A., 2017. Carte hydrogéologique de Wallonie, Planchettes Binche – Morlanwelz n° 46/5-6. (Hydrogeological Map of Wallonia).

Bougard, G., Roland, S., Rorive, A., 2017. Carte hydrogéologique de Wallonie, Planchettes Quiévrain – Saint-Ghislain n° 45/5-6. (Hydrogeological Map of Wallonia).

Canter, L.W., 2019. Nitrates in groundwater. Routledge.

Christiaens, L., Orban, P., Brouyère, S., Goderniaux, P., 2023. Tracking the sources and fate of nitrate pollution by combining hydrochemical and isotopic data with a statistical approach. Hydrogeology Journal 31, 1271–1289. https://doi.org/10.1007/s10040-023-02646-1

Clement, T.P., 1999. A modular computer code for simulating reactive multi-species transport in 3-dimensional groundwater systems. Pacific Northwest National Lab.(PNNL), Richland, WA (United States).

Craswell, E., 2021. Fertilizers and nitrate pollution of surface and ground water: an increasingly pervasive global problem. SN Applied Sciences 3, 518.

Dassargues, A., 2018. Hydrogeology: groundwater science and engineering. CRC Press.

Di, H.J., Cameron, K.C., 2002. Nitrate leaching in temperate agroecosystems: Sources, factors and mitigating strategies. Nutrient Cycling in Agroecosystems 64, 237–256. https://doi.org/10.1023/A:1021471531188

Dupont, N., 2021. Analyse de la structure du socle paléozoïque hainuyer. Implications sur les propriétés des réservoirs profonds. (Structural analysis of the Hainaut Paleozoic basement: implications for deep reservoir properties) (Phd Thesis). Université de Mons, Polytech Mons Faculty, Mons.

EEA, C., 2018. Corine Land Cover (CLC) 2018, Version 2020_20u1.

Eltarabily, M.G., Negm, A.M., Yoshimura, C., Saavedra, O.C., 2017. Modeling the impact of nitrate fertilizers on groundwater quality in the southern part of the Nile Delta, Egypt. Water Science and Technology: Water Supply 17, 561–570.

Erisman, J.W., Galloway, J.N., Seitzinger, S., Bleeker, A., Dise, N.B., Petrescu, A.R., Leach, A.M., de Vries, W., 2013. Consequences of human modification of the global nitrogen cycle. Philosophical Transactions of the Royal Society B: Biological Sciences 368, 20130116.

Fan, A.M., Steinberg, V.E., 1996. Health Implications of Nitrate and Nitrite in Drinking Water: An Update on Methemoglobinemia Occurrence and Reproductive and Developmental Toxicity. Regulatory Toxicology and Pharmacology 23, 35–43. https://doi.org/10.1006/rtph.1996.0006

Fettweis, X., Franco, B., Tedesco, M., Van Angelen, J., Lenaerts, J.T., van den Broeke, M.R., Gallée, H., 2013. Estimating the Greenland ice sheet surface mass balance contribution to future sea level rise using the regional atmospheric climate model MAR. The Cryosphere 7, 469–489.

Focaccia, S., Panini, G., Pedrazzoli, P., Ciriello, V., 2021. A meta-modeling approach for hydrological forecasting under uncertainty: Application to groundwater nitrate response to climate change. Journal of Hydrology 603, 127173.

Gouvernement Wallon, 2016. Code de l'Eau, Annexe XIV, [A.G.W. 03.05.2007] [A.G.W. 12.02.2009], Evaluation de la qualité des masses d'eau souterraine. (Water Legislation. Assessment of Groundwater Body Quality)

Habils, F., Roland, S., Rorive, A., 2017a. Carte hydrogéologique de Wallonie, Planchettes Jurbise – Obourg n° 45/3-4. (Hydrogeological Map of Wallonia).

Habils, F., Roland, S., Rorive, A., 2017b. Carte hydrogéologique de Wallonie, Planchettes Beloeil – Baudour n° 45/1-2. (Hydrogeological Map of Wallonia).
Hérivaux, C., Orban, P., Batlle-Aguilar, J., Brouyère, S., Goderniaux, P., 2008. Socio-economic analysis integrating soil-water system modelling for the Geer catchment (Meuse, Walloon region) - diffuse nitrate pollution in groundwater. (No. I3.8). AquaTerra.
IDEA, 2015. CHYDRO-004 – Délimitation des zones de prévention du puits BRASSICO à GHLIN (MONS). (Delineation of the Protection Zones for the BRASSICO Well in GHLIN)
Karlović, I., Posavec, K., Larva, O., Marković, T., 2022. Numerical groundwater flow and nitrate transport assessment in alluvial aquifer of Varaždin region, NW Croatia. Journal of Hydrology: Regional Studies 41, 101084.
Langevin, C.D., Hughes, J., Banta, E., Provost, A., Niswonger, R., Panday, S., 2017a. MODFLOW 6, the US Geological survey modular hydrologic model. US Geological Survey. https://doi.org/10.5066/F76Q1VQV.
Langevin, C.D., Hughes, J.D., Banta, E.R., Niswonger, R.G., Panday, S., Provost, A.M., 2017b. Documentation for the MODFLOW 6 Groundwater Flow Model (Report No. 6-A55), Techniques and Methods. Reston, VA. https://doi.org/10.3133/tm6A55
Langevin, C.D., Hughes, J.D., Provost, A.M., Russcher, M.J., Panday, S., 2024. MODFLOW as a Configurable Multi-Model Hydrologic Simulator. Groundwater 62, 111–123.
Langevin, C.D., Provost, A.M., Panday, S., Hughes, J.D., 2022. Documentation for the MODFLOW 6 groundwater transport model (No. 2328–7055). US Geological Survey.
Lee, M.-S., Lee, K.-K., Hyun, Y., Clement, T.P., Hamilton, D., 2006. Nitrogen transformation and transport modeling in groundwater aquifers. Ecological modelling 192, 143–159.
Marliere, R., 1967. Carte géologique de la Belgique à l'échelle 1/25.000. Texte Explicatif de la Feuille Mons-Givry. (Geological Map of Belgium at 1:25000 Scale. Explanatory Text for the Mons-Givry Sheet)
McDonald, M.G., Harbaugh, A.W., 1988. A modular three-dimensional finite-difference ground-water flow model. US Geological Survey.
Mengeot, A., Roland, S., Rorive, A., 2017a. Carte Hydrogéologique, Mons - Givry, 45 7/8, Notice explicative. (Hydrogeological Map of Wallonia, Explanatory Text)
Mengeot, A., Roland, S., Rorive, A., 2017b. Carte hydrogéologique de Wallonie, Planchettes Mons – Givry n° 45/7-8. (Hydrogeological Map of Wallonia)
O'Neill, B.C., Tebaldi, C., Van Vuuren, D.P., Eyring, V., Friedlingstein, P., Hurtt, G., Knutti, R., Kriegler, E., Lamarque, J.-F., Lowe, J., 2016. The scenario model intercomparison project (ScenarioMIP) for CMIP6. Geoscientific Model Development 9, 3461–3482.
Orban, P., Brouyère, S., Batlle-Aguilar, J., Couturier, J., Goderniaux, P., Leroy, M., Maloszewski, P., Dassargues, A., 2010. Regional transport modelling for nitrate trend assessment and forecasting in a chalk aquifer. Journal of contaminant hydrology 118, 79–93.
Paradis, D., Vigneault, H., Lefebvre, R., Savard, M.M., Ballard, J.-M., Qian, B., 2016. Groundwater nitrate concentration evolution under climate change and agricultural adaptation scenarios: Prince Edward Island, Canada. Earth System Dynamics 7, 183–202.
Pirson, S., Spagna, P., Baele, J.-M., Damblon, F., Gerrienne, P., Vanbrabant, Y., Yans, J., 2008. An overview of the Geology of Belgium. Memoirs of the Geological Survey of Belgium 55, 5–25.
Rorive, A., 1983. Détermination des ressources souterrains de la nappe du Crétacé de la Vallée de la Haine (Assessment of Groundwater Resources of the Cretaceous Aquifer in the Haine Valley). FPMs (UMONS-IDEA).
Rorive, A., Goderniaux, P., 2014. L'aquifère du Crétacé de la vallée de la Haine (The Cretaceous Aquifer of the Haine Valley), in: Dassargues, A., Walraevens, K. (Eds.), Watervoerende Lagen En Grondwater in België / Aquiferes et Eaux Souterraines En Belgique (Aquifers and Groundwater in Belgium). Gent : Academia press.
Rorive, A., Van Wittenberge, F., 2004. PIRENE, Programme Intégré de Recherche Environnement-Eau, Caractérisation et modélisation des nappes d'eau souterraine, Novembre 2000 - Octobre 2004 (Rapport Final) (Integrated Environment-Water Research Program: Characterization and Modelling of Groundwater Resources - Final Report). Faculté Polytechnique de Mons, Cellule Hydrogéologie.

928 Rotiroti, M., Sacchi, E., Caschetto, M., Zanotti, C., Fumagalli, L., Biasibetti, M., Bonomi, T., Leoni, B.,
929 2023. Groundwater and surface water nitrate pollution in an intensively irrigated system:
930 Sources, dynamics and adaptation to climate change. Journal of Hydrology 623, 129868.
931 Sandor, J., Kiss, I., Farkas, O., Ember, I., 2001. Association between gastric cancer mortality and nitrate
932 content of drinking water: ecological study on small area inequalities. European Journal of
933 Epidemiology 17, 443–447.
934 Sarkar, S., Mukherjee, A., Senapati, B., Duttagupta, S., 2022. Predicting potential climate change
935 impacts on groundwater nitrate pollution and risk in an intensely cultivated area of South Asia.
936 ACS Environmental Au 2, 556–576.
937 Singh, B., Sekhon, G., 1979. Nitrate pollution of groundwater from farm use of nitrogen fertilizers—A
938 review. Agriculture and Environment 4, 207–225.
939 Smith, V.H., Tilman, G.D., Nekola, J.C., 1999. Eutrophication: impacts of excess nutrient inputs on
940 freshwater, marine, and terrestrial ecosystems. Environmental pollution 100, 179–196.
941 Sohier, C., Degre, A., 2021. Développements complémentaires du modèle EPICgrid (Supplementary
942 Developments of the EPICgrid Model).
943 Sohier, C., Degre, A., 2016. Modélisation prospective des impacts des pratiques agricoles sur la qualité
944 du cycle de l'eau en Wallonie « Programme de recherche AQUAMOD » (Prospective Modelling
945 of the Impacts of Agricultural Practices on the Water Cycle Quality in Wallonia: « AQUAMOD
946 Research Program »).
947 Sohier, C., Degre, A., 2010. Modelling the effects of the current policy measures in agriculture: An
948 unique model from field to regional scale in Walloon region of Belgium. Environmental Science
949 & Policy 13, 754–765.
950 Sohier, C., Degre, A., Dautrebande, S., 2009. From root zone modelling to regional forecasting of nitrate
951 concentration in recharge flows–The case of the Walloon Region (Belgium). Journal of
952 hydrology 369, 350–359.
953 Spalding, R.F., Exner, M.E., 1993. Occurrence of nitrate in groundwater - A review. Journal of
954 Environmental Quality 22, 392–402.
955 https://doi.org/10.2134/jeq1993.00472425002200030002x
956 SPW, Ressources naturelles et Environnement, 2019. Banque de données "10-sous."
957 SPW, DEE, DESO, 2022. Etat des nappes et des masses d'eau souterraine de Wallonie (Status of
958 Groundwater Bodies in Wallonia). SPW, Wallonia, Belgium.
959 Strebel, O., Duynisveld, W., Böttcher, J., 1989. Nitrate pollution of groundwater in western Europe.
960 Agriculture, ecosystems & environment 26, 189–214.
961 Stuart, M., Gooddy, D., Bloomfield, J., Williams, A., 2011. A review of the impact of climate change on
962 future nitrate concentrations in groundwater of the UK. Science of the Total Environment 409,
963 2859–2873.
964 SWDE, 2002. Rapport technique n°149. Réalisation de six puits de reconnaissance (PR1 à PR6) dans le
965 cadre de l'étude des zones de prévention des prises d'eau "Givry P1 et Givry P2" à Quévy (anct.
966 Givry) (Technical Report No. 149: Construction of six exploration wells (PR1 to PR6) as part
967 of the study on protection zones for the "Givry P1 and Givry P2" wells in Quévy).
968 van der Maaten, L.J.P., Hinton, G.E., 2008. Visualizing High-Dimensional Data Using t-SNE. Journal
969 of Machine Learning Research 9, 2579–2605.
970 Vitousek, P.M., Aber, J.D., Howarth, R.W., Likens, G.E., Matson, P.A., Schindler, D.W., Schlesinger,
971 W.H., Tilman, D.G., 1997. Human alteration of the global nitrogen cycle: Sources and
972 consequences. Ecological Appplications 7, 737–750. https://doi.org/10.1890/1051-
973 0761(1997)007[0737:HAOTGN]2.0.CO;2
974 Wei, X., Bailey, R.T., Records, R.M., Wible, T.C., Arabi, M., 2019. Comprehensive simulation of nitrate
975 transport in coupled surface-subsurface hydrologic systems using the linked SWAT-
976 MODFLOW-RT3D model. Environmental Modelling & Software 122, 104242.
977 https://doi.org/10.1016/j.envsoft.2018.06.012
978 WHO, 2017. Guidelines for drinking-water quality: Fourth edition incorporating the first addendum.
979 World Health Organization.
980 Williams, J., Singh, V., 1995. The EPIC model. Computer models of watershed hydrology. Water Resour.
981 Publ. Highl. Ranch Colo 25, 909–1000.

Wyard, C., Scholzen, C., Fettweis, X., Van Campenhout, J., François, L., 2017. Decrease in climatic conditions favouring floods in the south-east of Belgium over 1959–2010 using the regional climate model MAR. International Journal of Climatology 37, 2782–2796.
Zhang, H., Yang, R., Wang, Y., Ye, R., 2019. The evaluation and prediction of agriculture-related nitrate contamination in groundwater in Chengdu Plain, southwestern China. Hydrogeology Journal 27, 785–799.

Declarations

Ethics approval

Not applicable

Consent to participate

Not applicable

Consent for publication

Not applicable

Availability of Data and Materials

The datasets generated during and/or analysed during the current study are not publicly available but are available from the corresponding author on reasonable request

Competing Interests

The authors declare they have no financial and non-financial interests.

Funding

This research was financially supported by SPGE (Société Publique de Gestion de l'Eau – Public Water Management Company), which is a public limited company set up by the Walloon Region.

Author Contributions

LC generated the results, did most of the writing and the layout of the contribution. PG was the main supervisor and motivator for the paper, contributed mostly to the redaction and writing part as well as assisted actively the modeling part. GV assisted actively the modeling part. AD and CS contributed to conceptual and methodological discussions and generated the EPIC GRID scenariost. PO contributed to conceptual and methodological discussions and helped with the writing part. SB contributed to conceptual and methodological discussions.